LIGHT SCATTERING STUDY ON SINGLE WALL CARBON NANOTUBE (SWNT) DISPERSIONS

A Thesis

Presented to

The Academic Faculty

by

Tong Wang

In Partial Fulfillment

of the Requirements for the Degree

Master of Science in the

School of Polymer, Textile and Fiber Engineering

Georgia Institute of Technology

April 2004

LIGHT SCATTERING STUDY ON SINGLE WALL CARBON NANOTUBE (SWNT) DISPERSIONS

Approved by:

Dr. Satish Kumar, Chairman

Dr. Mohan Srinivasarao

Dr. Rina Tannenbaum

Dr. Tao Liu

Date Approved April, 8 th, 2004

ACKNOWLEDGEMENTS

First, I would like to thank my advisor, Dr. Satish Kumar for his guidance, encouragement and support during this research. In addition, I would like to thank Dr. Rina Tannenbaum, who kindly let me use the light scattering instrument, and also for serving on my thesis committee. I also would like to thank Dr. Morhan Srinivasarao for serving on the thesis committee. I would like to thank Dr. Tao Liu for his insightful suggestions and helpful discussions and for serving on the thesis committee.

I would like to thank Dr. Tetsuya Uchida for the transmission electron microscopy study. Thanks to Dr. Sreekumar Veedu for SWNT oluem dispersions and to Valerie Moore at Rice University for PVP wrapped SWNT aqueous dispersions. I also appreciated the help of all my group members. Finally, I would like to express my deepest gratitude to my parents and to my family for their support and encouragement.

TABLE OF CONTENTS

LIST OF TABLES

LIST OF FIGURES

SUMMARY

Carbon nanotubes, and particularly single wall carbon nanotubes (SWNTs) have attracted much attention for their unique structure, as well as for their excellent mechanical, electrical and thermal properties. Most properties of carbon nanotubs are closely related with their anisotropic structure and geometry factor. Characterization of carbon nanotube length is critical for understanding their behavior in solutions as well as in polymer composites. Microscopy, particularly atomic force microscopy, has been used for their length measurement. Microscopy, though straightforward, is quite laborious, particularly for statistically meaningful sampling.

Light scattering can be used to measure particle dimensions. In this study, light scattering has been used to study polyvinyl pyrrolidone (PVP) wrapped SWNTs surfactant assisted aqueous dispersion and SWNT dispersion in oleum. To determine the length of SWNTs, Stokes - Mueller formalism was used, which is a universal model for particles with any size and shape. The Mueller matrix for an ensemble of long, thin cylinders proposed by McClain et al. was used in this study. This Mueller matrix includes the information of size (length and radius) and optical constants (refractive index and extinction coefficient) of cylinders. In this matrix, extinction coefficient, radius and length of SWNTs are unknown. By normalizing scattering intensity I_θ (θ from 30 to 155°) to that at 30°, the effects of radius and extinction coefficient were cancelled out. Thus, the effect of SWNT length on scattering intensity could be studied independently. A series of curves of normalized scattering intensity of SWNTs ($I_\theta/I_{30°}$) with varied lengths as a function of wave vector were predicted. A curve of normalized scattering intensity of SWNT as a function of wave vector was also obtained experimentally. By comparing

experimental and predicted curves, average SWNT length in the dispersion has been determined.

Scattering intensity at a given angle initially increases with concentration, and then reaches a critical concentration(C*), above which the scattering intensity decreases. This phenomenon has been attributed to the competition between scattering and absorption of light by the presence of SWNT. By using Beer-Lambert law, this phenomenon has been used to determine the molar absorption coefficient of SWNTs.

CHAPTER 1

INTRODUCTION

Carbon nanotubes have been the focus of considerable research since their discovery in 1991. They combine exceptional mechanical, thermal and electrical properties. They have high modulus, stronger than steel, thermally stable up to 2800°C in vacuum, thermal conductivity is twice that of diamond, and the electric - current - carrying capacity is 1000 times higher than that of copper wire.[1] All of these properties open up the broad application areas for carbon nanotubes.

Some of the excellent properties of carbon nanotubes are a result of their high aspect ratio. The carbon nanotubes have long cylindrical structure with diameter at nm level and length at μm level, which makes their aspect ratio as high as 1000 or larger. The aspect ratio has significant effect on the properties of carbon nanotubes and their composites, which has been investigated theoretically and experimentally. Young' modulus of carbon nanotubes for axial deformation was studied by use of a nonorthogonal tight binding formalism. The results show that the modulus depends on the diameter when the tubes are small (<1.2 nm); [2] The dependence of torsion stiffness K of carbon nanotubes on the radius (R) and length (L) of tubes is found to be as $K \propto R^3 / L^2$.[3] In carbon nanotubes reinforced polymer composites, geometry also plays an important role. It is believed that high aspect ratio of carbon nanotubes provides large surface area for efficient load transfer,[4] indicating high performance that the carbon nanotube composites can achieve. As reported in Kumar et al's paper, better exfoliation and smaller diameter of SWNT ropes would result in PAN/SWNT composite fibers with higher modulus.[5] Allaoui et al. experimentally investigated the effect of the length and size of MWNTs on the mechanical properties and electrical properties of MWNT/epoxy

composites. They reported that length of MWNTs has a dominant role in improving the electrical conductivity. Regarding the mechanical properties of composites, good exfoliation and appropriate aspect ratio are important. [6]

All of these studies bring our concern to the geometry of carbon nanotubes. Several methods have been explored in measuring diameter and length of carbon nanotubes. Microscopic techniques such as scanning electron microscopy, transmission electron microscopy and atomic force microscopy have been used.[7] [8] The advantage of microscopic techniques is straightforward. However, these microscopic techniques are quite laborious, particularly for statistically meaningful sampling. Also, if the carbon nanotubes form very long bundles, it would be hard to follow their ends, and measure the length accurately.

The objective of this study is to find a reliable method to measure the length of carbon nanotubes. Light scattering is used to measure the particle size no matter what shape it is, leading us to consider its use to measure the length of SWNTs. In this study, light scattering was applied to SWNT dispersions to study their scattering behavior. The scattering intensities as a function of angle or as a function of concentration were measured. On the other hand, the scattering curve of SWNT was simulated by Stokes-Mueller formalism, in which the incident beam is transformed into scattered beam by a matrix-Mueller matrix. McClain model, which provides Mueller matrix for long, thin cylinder ensemble was used in this study, [9] the relationship between incident beam and scattered beam was set up, and a scattering curve of SWNTs was simulated. From a comparison of the simulated curves with experimental curves, average SWNT length was determined. Based on the atomic structure, molecular weight of SWNTs was calculated with length obtained from light scattering and diameter obtained from AFM. Molar absorption coefficient of SWNT dispersion was also determined by fitting the scattering data with Beer-Lambert law.

CHAPTER 2

LITERATURE REVIEW

2.1 Discovery of carbon nanotubes

Carbon nanotubes were discovered in 1991 by the Japanese electron microscopist Sumio Iijima who was studying the material deposited on the cathode during the arc - evaporation synthesis of fullerenes. He found that the central core of the cathodic deposit contained a variety of closed graphitic structures including nanoparticles and nanotubes, with outer diameters of 4 - 30 nm and length of 1 μm.[10] Since these tubes consisted of multiple shells, where many tubes are arranged in a coaxial fashion, and tube diameter is of the order of nanometers, he called these tubes multi - wall nanotubes (MWNTs) (Figure 2.1).

In 1993, single - wall nanotubes (SWNTs), which are seamless cylinders each made of a single graphite sheet, were reported.[11] Their diameters range from 0.4 to 3 nm, and lengths are of the order of micrometers (Figure 2.2). SWNTs tend to come together to form bundles, while isolated or single tubes are also present.

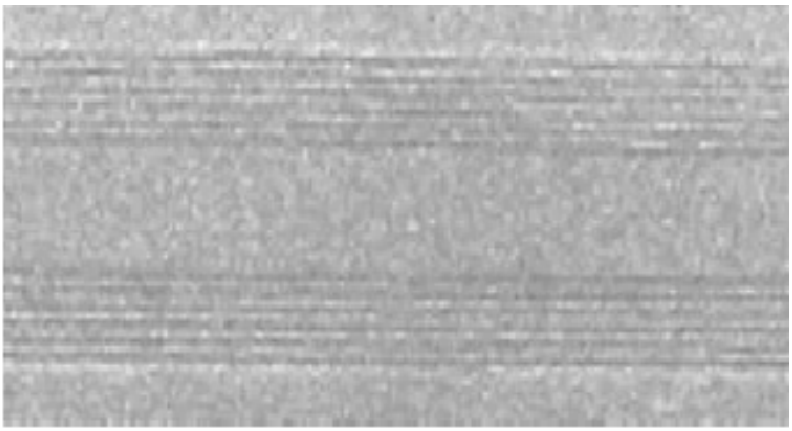

Figure 2.1. MWNT[12]

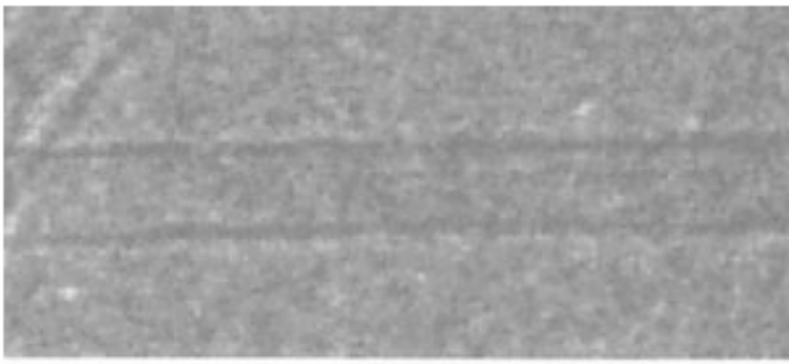

Figure 2.2 SWNT [12]

2.2 Atomic structure of carbon nanotubes

Carbon nanotubes can be essentially thought of as a layer of graphite rolled - up into a cylinder. The atomic structure of nanotube is described in terms of tube chirality, which is defined by chiral vector $\vec{C}_h$ and chiral angle θ (Figure 2.3[13]). The chiral vector $\vec{C}_h$ is given by the following equation:

$$\vec{C}_h = n\vec{a}_1 + m\vec{a}_2$$

Where the integers n, m are the number of steps along the zig - zag carbon bonds of the hexagonal lattice, $\vec{a}_1$ and $\vec{a}_2$ are unit vectors shown in Figure 2.3. Along $\vec{C}_h$, the graphite sheet is rolled into a tubular form. The chiral angle determines the amount of "twist" in the tube. Depending on chiral angle θ, various types carbon nanotubes can form. If θ = 0° (n = 0 or m = 0), the nanotube is a "zig - zag" tube; If θ = 30° (n = m), the nanotube is an "armchair" tube; If θ is between 0 and 30° (n ≠ m), the nanotube is a chiral tube (Figure 2.4). The chirality of the carbon nanotube has significant implications on the material properties, especially on electronic properties of carbon nanotube. Depending on chirality, carbon nanotube can be either metallic or semi conducting. [14] The geometry parameters of carbon nanotubes are given in Table 2.1.

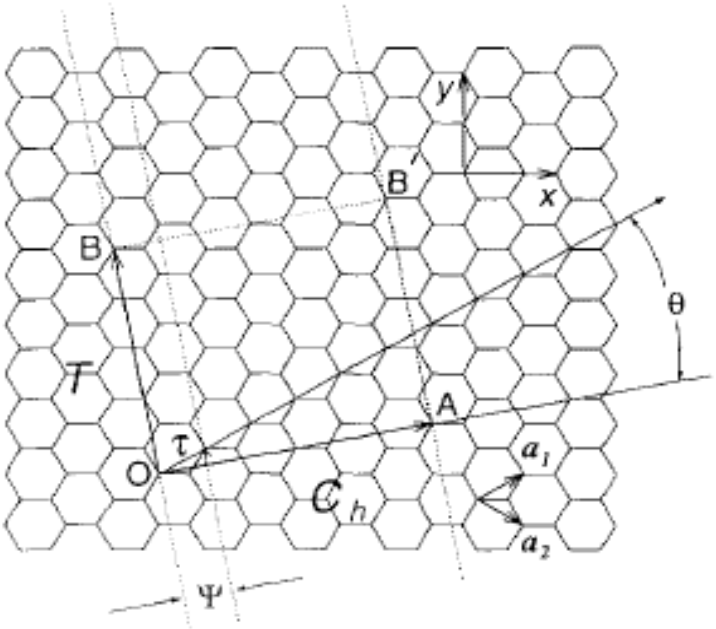

Figure 2.3 2D graphite sheet of carbon nanotube. The chiral vector OA is defined as: $\vec{C}_h = n\vec{a}_1 + m\vec{a}_2$ on the honeycomb lattice by unit vectors a_1 and a_2, and the chiral angle θ is defined with respect to the zig - zag axis. Along the zig - zag axis θ = 0; also shown are the lattice vector OB = T of the 1D tubule unit cell, and the rotational angle ψ and the translation τ which constitute the basic symmetry operation R = (ψ | τ)[13]

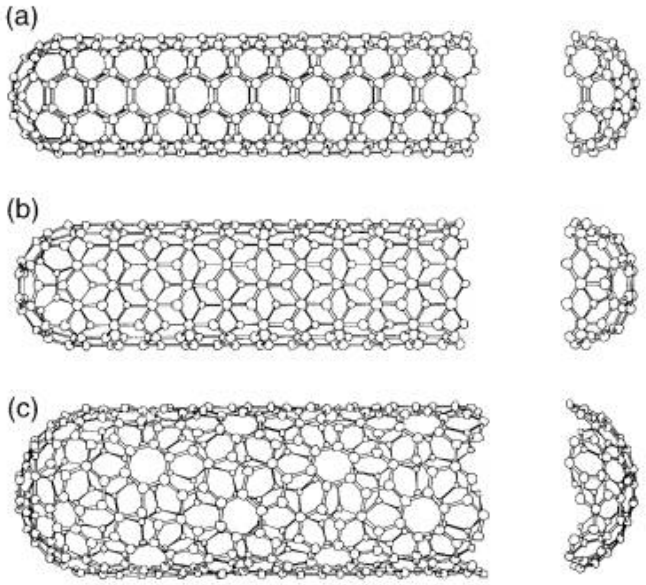

Figure 2.4 Three types of carbon nanotubes[13]
a: arm chair; b: zig - zag; c: chiral tube

Table 2.1 Geometry parameters of carbon nanotubes (adapted from [13])

Symbol	Name	Formula	Value
$a_{c\text{-}c}$	Carbon-carbon distance		1.421Á(graphite)
a	Length of unit vector	$\sqrt{3}a_{c-c}$	2.46 Á
a_1, a_2	Unit vectors	$(\frac{\sqrt{3}}{2},\frac{1}{2})a, (\frac{\sqrt{3}}{2},-\frac{1}{2})a$	in (x, y) coordinates
C_h	Chiral vector	$C_h = na_1+ma_2 \equiv (n,m)$	n, m: integers
L	Circumference of nanotube	$L = \left\|C_h\right\| = a\sqrt{n^2+m^2+nm}$	$0 \le \left\|m\right\| \le n$
d_t	Diameter of nanotube	$d_t = \frac{L}{\pi} = \frac{\sqrt{n^2+m^2+nm}}{\pi}a$	
θ	Chiral angle	$\sin\theta = \frac{\sqrt{3}m}{2\sqrt{n^2+m^2+nm}}$ $\cos\theta = \frac{2n+m}{2\sqrt{n^2+m^2+nm}}$ $\tan\theta = \frac{\sqrt{3}m}{2n+m}$	$0 \le \left\|\theta\right\| \le 30^0$
d	The highest common divisor of (n, m)		
d_R	The highest common divisor of (2n+m, 2m+n)	$d_R = \begin{cases} d, \text{if } n-m \text{ not a multiple of } 3d \\ 3d, \text{if } n-m \text{ a multiple of } 3d \end{cases}$	
$\vec{T}$	Translational vector of 1D unit cell	$\mathbf{T} = t_1a_1+t_2a_2 \equiv (t_1,t_2)$ $t_1 = \frac{2m+n}{d_R}$ $t_2 = \frac{2n+m}{d_R}$	t_1, t_2: integers
T	Length of $\vec{T}$	$T = \frac{\sqrt{3}L}{d_R}$	
N	Number of hexagons per 1D unit cell	$N = \frac{2(n^2+m^2+nm)}{d_R}$	$2N \equiv n_C/\text{unit cell}$

2.3 Properties of carbon nanotubes

2.3.1 Mechanical properties of carbon nanotubes

Carbon nanotubes have high strength and stiffness, which open broad application areas in high performance composites. SWNTs have much higher tensile strength and modulus than carbon fibers and PBO zylon, and lower density (Table 2.2).

Table 2.2 Mechanical properties of SWNT, carbon fiber and zylon^{TM} fiber

Properties	SWNT[15]	carbon fiber[16]	PBO zylon ^{TM} HM[17]
Tensile strength GPa	~ 37	~ 4	5.8
Tensile Modulus GPa	~ 640	~ 400	270
Elongation at break %	~ 5.8	~ 2.0	2.5
Density g/cm^3	~ 1.3	~ 1.75	1.56

2.3.2 Electrical and electronic properties of carbon nanotubes

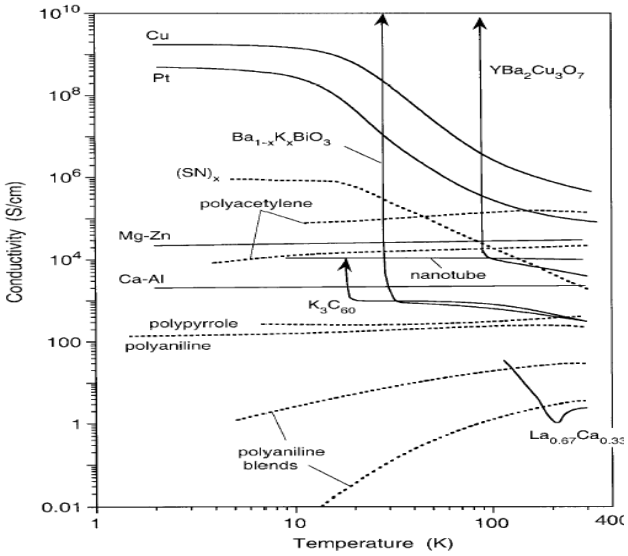

Figure 2.5 Conductivity of carbon nanotubes and conducting polymers as a function of temperature.[18]

Carbon nanotubes have very high electrical conductivity. The conductivity of SWNT is much higher than those of conductive polymers, which is about 10^4 S/cm[18].

2.3.3 Thermal properties of carbon nanotubes

Comparable to thermal conductivity of a hypothetical isolated graphene monolayer or diamond, carbon nanotubes have an unusually high value, about 6600 W/m·K at room temperature. The thermal conductivity of carbon nanotubes as a function of temperature is given in Figure 2.6. It can be seen that temperature has significant effect on thermal conductivity of carbon nanotubes. Thermal conductivity is highest at about 100 K.[19]

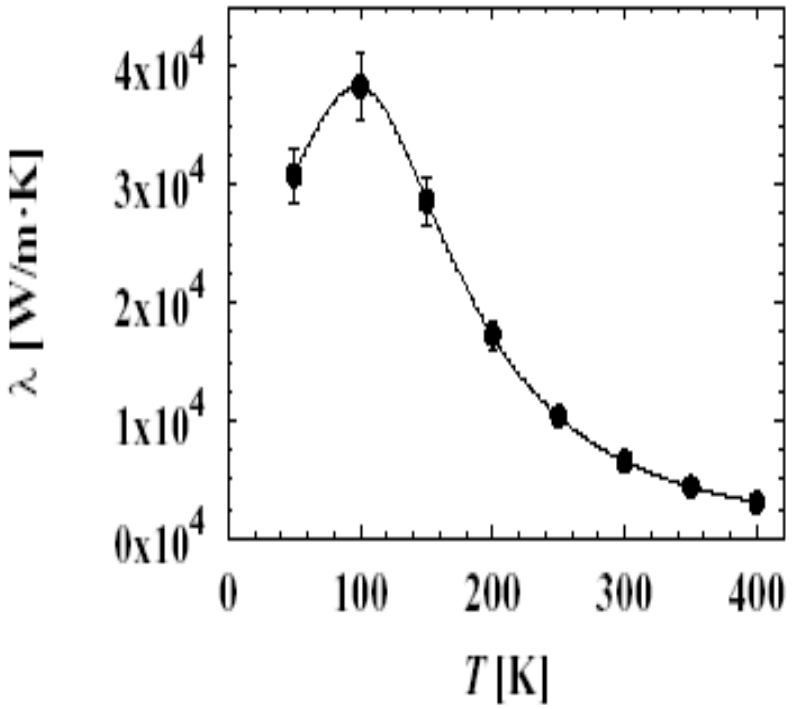

Figure 2.6 Temperature dependence of the thermal conductivity for a (10, 10) carbon nanotube for temperatures below 400 K.[19]

2.4 Applications of carbon nanotubes

The excellent mechanical, electrical and thermal properties of carbon nanotubes ensure their wide applications in electrical, optical and mechanical fields.

2.4.1 High performance materials

The mechanical properties of polymers can be greatly enhanced by the addition of carbon nanotubes. Composites can achieve high mechanical properties if load can be effectively transferred from the matrix to the nanotubes. Rantell et al. reported that with only the addition of 1 wt% nanotubes, the elastic stiffness of carbon nanotube/PS is increased by 36 to 42 % and tensile strength increased by 25 % compared to PS.[20] Kumar et al. found that poly(vinyl alcohol) (PVA) composite films using poly(vinyl pyrrolidone) (PVP) and sodium dodecyl sulfate (SDS) covered, well dispersed SWNTs exhibit significant improvement in tensile strength and modulus as compared to the control PVA and PVA/PVP/SDS films.[21] Sreekumar et al. reported that solution spun PAN/SWNT fiber containing 10 wt % SWNT exhibited 100 % increase in tensile modulus at room temperature and an order of magnitude increase at 150 ˚C, significant reduction of thermal shrinkage and polymer solubility, and a 40 ˚C increase in glass transition temperature as compared to the control PAN fiber.[5]

2.4.2 Field emission displays

Carbon nanotubes are also possible candidates for next generation display devices such as field emission device (FED). FED is to add a high electric field to a wire in order to produce electrons. Strength of the electric field and the geometry of the wire determine the efficiency of generating electrons.[22] Large field amplification requires both high electric field and sharp radius of wire. Carbon nanotubes exhibit both of these properties, and are a good candidate for this application.

2.4.3 Nanotube sensors

The electrical resistance of semiconducting SWNTs changes dramatically when exposed to gaseous molecules. This unusual property makes them useful for chemical sensors. Nanotubes act as the wire between two electrodes so that changes in conductance can be measured.[23]

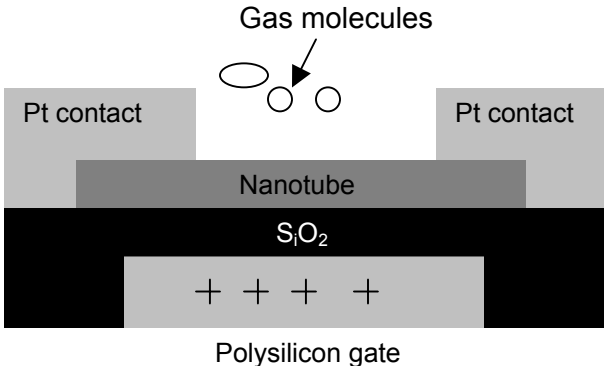

Figure 2.7 Schematic of nanotube sensor.[23]

2.4.4 Lighting elements

Nanotubes are excellent electron source for creation of lighting elements. The electrons produced by nanotubes are used to bombard a surface coated with phosphor in order to produce light. The brightness of this light is usually 2 times brighter than conventional lighting elements (due to the high electron efficiency).[24]

2.4.5 Fuel cells and secondary cells

If hydrogen is used as fuel cell instead of petroleum, much higher energy can be generated and no environmental problem occurs. But the storage of hydrogen is a problem because large bath is needed. The problem can be solved by use of carbon nanotubes. Hydrogen can condense inside narrow carbon nanotubes physically and chemically. Physisorption of hydrogen occurs in carbon nanotubes by trapping hydrogen molecules inside the cylindrical structure of the nanotubes or by trapping

hydrogen in the interstitial sites between nanotubes; Chemisorption occurs by hydrogen dissociation and reaction with carbon nanotubes. The high hydrogen uptake ability of carbon nanotube suggests that it might be an effective hydrogen storage material for fuel - cell electric vehicles.[25]

2.4.6 Probe tips

The feature resolution obtained by AFM is determined largely by the size and shape of the probe tips.[26, 27] The commercially available tips place significant constraints on potential lateral resolution, and their shape restricts the ability of accessing narrow and deep features. These problems can be solved by attaching carbon nanotube to the ends of s_i tips.[28] The high aspect ratio nanotube tips are good at probing deep crevices and steep features. Additionally, the ability of carbon nanotube to elastically buckle limits the maximum force applied to a sample, which can prevent damage to delicate organic and biological samples, and makes the tips robust.[29] Nanotube tips can also be covalently functionalized at their ends to create chemically and biologically sensitive probes.

2.5 Effect of geometry factor on carbon nanotube properties and applications

2.5.1 Effect of geometry factor on carbon nanotubes properties

The highly anisotropic structure determines that carbon nanotubes have superior properties. Studies show that the mechanical properties of carbon nanotubes are closely related with their geometry. The modulus of carbon nanotubes is widely investigated by theoretical calculations and experimental methods. For axial deformation, Rubio et al. studied Young's modulus of carbon nanotube based on atomic interactions modeled by nonorthogonal tight-binding method. It is reported that for smaller diameter tubes, Young's modulus greatly increases with the diameter (diameter

< 1.2 nm); while for larger diameter tubes, the dependence is not significant (Figure 2.8).[2] The dependence of Young's modulus on diameter can be explained that smaller diameter of tubes causes higher curvature, and results in weaker bond, therefore lower Young's modulus. Molecular dynamics simulations with Tersoff-Brenner potential show that when carbon nanotube undergoes bending, stiffness K scales as diameter $D^{2.93}$ (Figure 2.9).[3] Wang et al. applied electrically induced force to study the bending Young's modulus of MWNTs, and observed that bending Young's modulus decreases significantly with diameter (Figure 2.10).[30] From continuum elastic theory, dependence of torsion stiffness K on radius R and length L is found to be $K \propto R^3/L^2$. Chen et al. studied torsion stiffness using the Tersoff-Brenner potential, and reported that $K \propto R^{3.01}$, which is in good agreement with the cubic dependence from continuum elastic theory (Figure 2.11).[3] All these results indicate that the properties of carbon nanotubes are closely related with their structure and geometry.

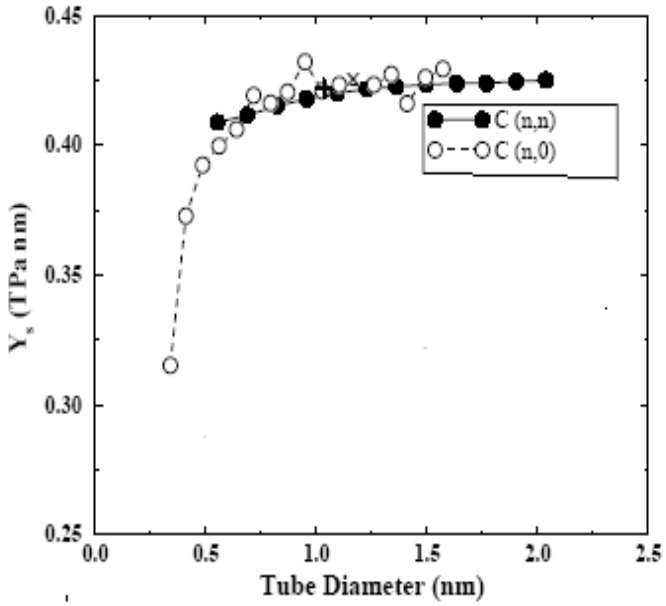

Figure 2.8 Young's modulus as a function of tube diameter (adapted from[2]).

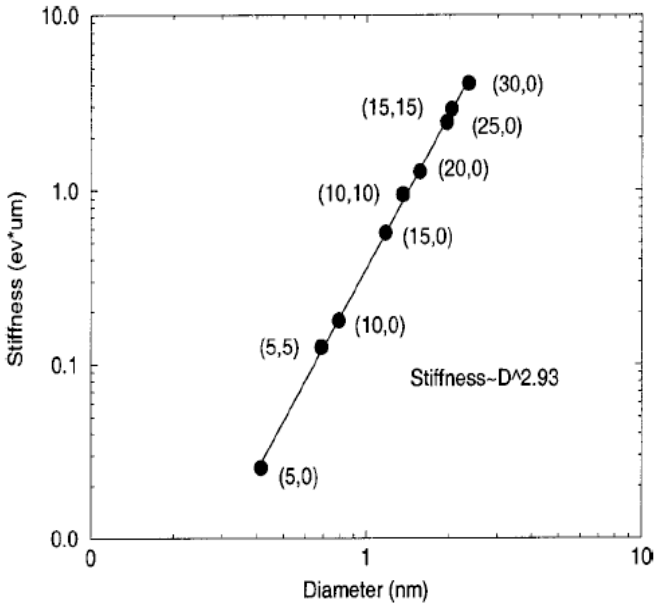

Figure 2.9 Bending stiffness as a function of tube diameter from molecular dynamic simulation with Tersoff-Brenner potential. [3]

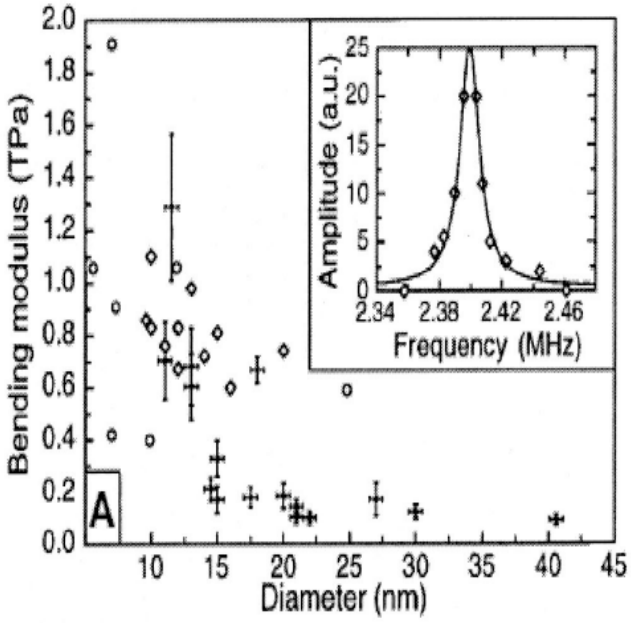

Figure 2.10 Bending modulus as a function of tube diameter. Solid circles are from Poncharal et al's paper;[30] others are from other experiments as referenced in Poncharal et al's paper.

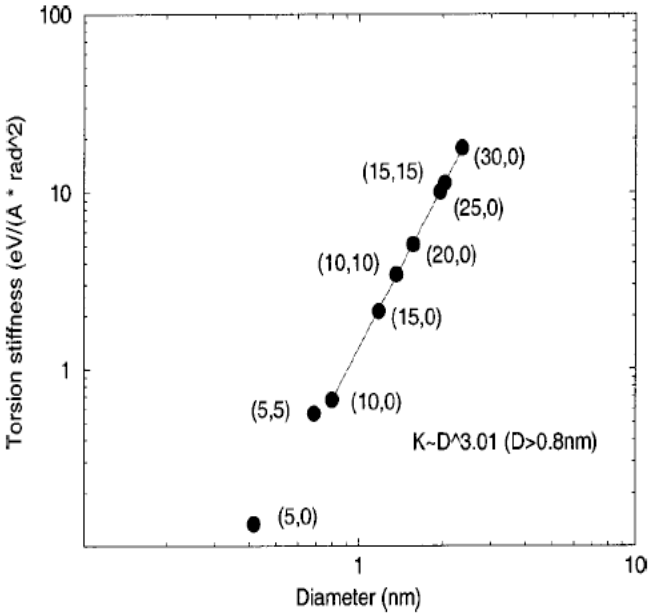

Figure 2.11 The torsion stiffness as a function of tube diameter for a series of zigzag and armchair SWNTs calculated with Tersoff-Brenner potential. The stiffness is scaled as $D^{3.01}$ for D< 0.8 nm.[3]

2.5.2 Effect of geometry factor on carbon nanotube applications

Geometry of carbon nanotubes is an important factor to be investigated in their applications. The aspect ratio of carbon nanotubes determines the mechanical properties of composites that they reinforce. High aspect ratio (length/diameter ~ μm/nm) and good dispersion of nanotubes in polymer matrix ensure large interfacial areas for stress transfer, which is much larger than that in short fiber reinforced composites.[4] In carbon nanotube reinforced composites, there is a critical aspect ratio, which is L/D $>\sigma_{max}/2\tau$, where σ_{max} is the maximum strength of carbon nanotubes, τ is the interfacial shear stress between the nanotubes and the polymer matrix. With a typical value of 50 MPa for the interfacial shear stress between nanotube and polymer matrix and 50 GPa for tensile strength of SWNTs, the critical aspect ratio is 50:1. For an optimum load transfer, the aspect ratio of carbon nanotubes should be at least 50:1.[3]

The importance of carbon nanotube aspect ratio can also be indicated in another application - scanning probe tip. The high aspect ratio of carbon nanotubes with small diameter and large length makes them ideal as scanning probe tips. Since the diameter of the scanning probe tip determines the imaging resolution, carbon nanotube tips can offer high resolution, while the length of CNT tips permits the tracing of rough surfaces with steep and deep features.[31] Another characteristic feature of nanotubes is that they can elastically buckle which makes them very robust and also prevents damage to delicate organic and biological samples by limiting the maximum force applied to the samples[29]. It is reported that carbon nanotube tip has longer life time and better resolution than s_i tip.[32]

2.6 Methods to measure the aspect ratio of carbon nanotubes

2.6.1 Common methods

By use of SEM, TEM, AFM and Raman spectroscopy, the diameter of carbon nanotube or bundles can be measured. The methods used for measuring length include AFM, TEM and SEM.[7,8] In Figure 2.12, length of an individual carbon naotube was measured by SEM.[7] Roth used chromatographic size separation (SEC) to fractionate SWNTs/water dispersion, and then measured the lengths of fractionated SWNTs by AFM and TEM.[8] Holmes reported a method that can be used to measure the length of pristine SWNTs by AFM. A “witness plate” was placed at different locations in the laser oven, the laser shutters were open for a short time, producing sparse nanotubes scattered on the substrates. If the exposure time is appropriate, individual SWNT can be distinguished on the plate, thus allowing AFM to measure its length without further processing.[33] SEM, TEM and AFM, though straightforward, are quite laborious, particularly for statistically meaningful sampling. When the nanotubes become longer, it

is impossible to follow them all the way to their ends. It is also hard to find the ends of tubes if they are buried in piles of nanoparticles. Thus these methods may be lower

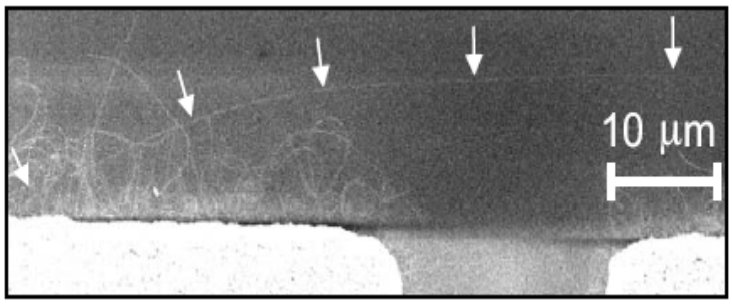

Figure 2.12 Scanning electron microspcoy of SWNT(Length is 60 µm)[7] .

estimation of the tube lengths. The other problem existing in these methods is that statistics on length is carried out locally, which may not reflect the whole length distribution in the sample. There is in urgent need for finding another method to measure the length of carbon nanotubes.

2.6.2 Light scattering method

2.6.2.1 Introduction of light scattering

In this study, light scattering was used to determine the length of SWNTs. Scattering of electromagnetic waves by any system is related to the heterogeneity of that system: Heterogeneity can be on the molecular scale or on the scale of aggregations of many molecules. If an obstacle, which could be a single electron, an atom or molecule, a solid or liquid particle, is illuminated by an electromagnetic wave, electric charges in the obstacle are set into oscillatory motion by the electric field of the incident wave. Accelerated electric charges radiate electromagnetic energy in all directions.[41] Light scattering is the basis for explaining why the sky is blue, why fog and emulsions are

opaque and other observations. It has been utilized in many areas of science to determine molecular weight, particle size, shape and diffusion coefficients etc.

The common phenomenon of light scattering can be used to obtain important information about the structure of the microscopic particles. When using light scattering to measure the properties of particles, solutions or dispersions are generally irradiated with a beam of laser light; and the scattered light is then measured using one or more detectors. The process is shown in Figure 2.13. In the technique known as static light scattering, the intensity of the scattered light is measured. This makes it possible to determine the molecular weight of the particles in the test sample, and that reveals how far the process of aggregation has progressed. If light intensity is measured from several scattering angles and the aggregates are large enough, it is possible to calculate the size of each aggregate. Depending on the particle size and shape, several light scattering models have been developed, which will be described in the following section.

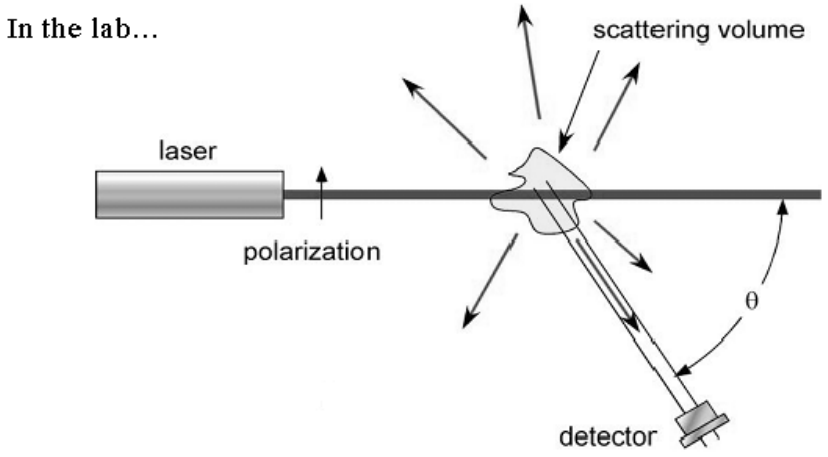

Figure 2.13 Schematic of the light scattering process.

2.6.2.2 Theory of static light scattering

To correlate scattering intensity with particle size and shape, several scattering models have been developed, which are described here. Each of them has its application range. Some of these models are described here.

- **Rayleigh scattering**

When the light is scattered by particles much smaller than the wavelength of the light (a << λ/10), Rayleigh scattering occurs, which treats the particles as though point scatterers. It occurs when light travels in transparent solids and liquids, but is most prominently seen in gases.Rayleigh scattering of sunlight from air molecules is the reason why sky appears blue to the human eyes (Lord Rayleigh, 1871). The amount of Rayleigh scattering is dependent upon the wavelength of the light; in particular, the dependence of scattering intensity on wavelength is $I_s \propto \frac{1}{\lambda^4}$ (I_s is scattering intensity, λ is wavelength). Therefore, shorter wavelength of light, stronger scattering it would have. Even though wavelength of violet is shorter than that of blue, we still see blue sky instead of violet sky. This is due to the effect of the eye being less sensitive to violet and the solar spectrum being somewhat depleted in violet, which provides a combined signal processed by the brain to yield the blue color of sky. [34]

- **Rayleigh – Debye - Gans scattering (RGD)**

Based on Rayleigh scattering, RGD theory was developed. In RGD scattering, the particle of arbitrary shape is subdivided into volume elements. Each element is treated as a Rayleigh scatterer, which is unperturbed by the presence of the rest of the particle. The fundamental approximation in RGD approach is that the " phase shift " corresponding to any points in the particle is negligible. Thus the internal field can be

approximated by the incident field. In case of low refractive index and small particle size, the following inequality is satisfied:

$$2ka\,(m-1)<1$$

k : propagation constant; for an undamped wave in a nonconducting media, $k = 2\pi/\lambda$;

λ: wavelength of light;

a: the longest dimension through the particle;

m: relative refractive index, ratio of refractive index of particles to refractive index of medium.

Scattering intensity I_s can be represented by:

$$I_s = (k^4 V^2/4\pi r^2)(m-1)^2 P(\theta)$$

$$P(\theta(= (1/V^2)\left|\int e^{i\delta} dV\right|^2$$

I_s: scattering intensity;

V: scattering volume;

r: radial distance;

P(θ): form factor.

Form factor P(θ) is dependent on particle size and shape. For random coil, thin disc, thin rod and sphere, P(θ) has different forms. Once I_s is detected, P(θ) corresponding a specific particle can be calculated, and particle size can be determined.

- **Mie scattering**

Mie theory provides rigorous solutions for light scattering by an isotropic sphere embedded in a homogeneous medium, homogeneous, dielectric sphere. It is applicable to spheres of all sizes, refractive indices and for radiation at all wavelengths.[48]

2.6.2.3 Scattering of carbon nanotubes

Carbon nanoutbes are long, thin and light absorptive cylindrical structure, which is beyond the application ranges of the light scattering models above. The theoretical model applying to SWNTs dispersion will be given in section of " THEORETICAL AND EXPERIMENTAL METHODS ". The light scattering works carried on carbon nanotube are briefly reviewed here. Most of these efforts are focused on studying the morphology of carbon nanotubes in dispersion. The approach they used is to investigate the fractal dimension, which can be detected by light scattering. It is found that scattering intensity has a power law dependence on wave vector q:[35]

$$I_s \sim q^{-D}$$

$q = 4\pi\sin(\theta/2)/\lambda$, D is fractal dimension. The morphology of fractal can be indicated by D value. The fractal dimension is 1 for rods, 2 for disks, and 3 for sphere.

Fischer et al. studied the dilute dispersion of individual SWNT in D_2O with added sodium dodecylbenzene sulfonate (SDS) by use of small angle neutron scattering (SANS). They found that the scattering intensity in the wave vector q range of $0.005 < q < 0.02$ Å^{-1} is characteristic of rigid rod, while the dependence of scattering intensity on q^{-2} was observed at $q \sim 0.004$ Å^{-1}, suggesting the existence of rod networks.[36] Their results seem inconsistent with other groups' work. In Dale W. Schaefer et al.'s paper, it was found that SWNTs exist as entangled network instead of rigid rods in polyelectrolyte dispersion based on small-angle (SAXS) and ultra-small angle X-ray (USAXS) scattering.[37]

In this study, we tried to determine the length of SWNTs by light scattering method. Rayleigh and RGD scattering theories are suitable for small and non-absorptive particles. Mie scattering is used for sphere. It is inappropriate to apply these models to SWNTs, which are long, thin, light absorptive cylinders. Specifically, a model for long, thin absorptive cylinder should be used.

CHAPTER 3

THEORETICAL AND EXPERIMENTAL METHODS

3.1 Materials

1. Polyvinyl pyrolidone (PVP) wrapped SWNT aqueous dispersion, provided by Rice University.
2. SWNTs (HiPCo), provided by CNI.
3. Oleum, free SO_3 content is 22 ~ 33 %, supplied by Aldrich.

3.2 Sample preparation

3.2.1 PVP wrapped SWNT aqueous dispersion

SWNT (HiPCo) powder was dispersed in 1 % sodium dodecyl sulfate (SDS) in water at a concentration of 46 mg/l by a combination of high - shear mixing and sufficient ultrasonication. Enough polyvinyl pyrolidone (PVP) was added to the mixture to make a 1 % solution by weight, which was then incubated at 50 °C for 12 h. Catalyst particles remaining from the SWNTs synthesis, residual SDS and polymer were removed by using centrifuge.[38]

PTFE filter with pore size 0.2 μm was used to filter deionized water. Original PVP wrapped SWNT aqueous dispersion was diluted to make a series of concentrations by addition of filtered water. These diluted dispersions were used for light scattering measurement.

3.2.2 SWNTs/oleum dispersion

The purified HiPCo SWNTs were vacuum - dried at 110 °C. Vacuum - dried purified SWNTs (0.125 g) were mixed in 50 g oleum (H_2SO_4, 30 % SO_3) in a glass flask

placed in a glovebox. The solution was stirred using a magnetic stirrer and maintained at 60 °C. Dry nitrogen gas flow was maintained in the glovebox. Original SWNTs/oleum dispersion was diluted to the desired concentration by addition of oleum. These diluted dispersions were used for light scattering measurement.[39]

3.3 Characterization

3.3.1 Light scattering technique

Light scattering measurement was carried out on BI - 200 SM Research Goniometer & Light Scattering System (Brookhaven Instrument Company). The incident beam is Helium - Neon laser with wavelength 633 nm. The instrument is shown in Figure 3.1. Static light scattering was carried out on SWNT dispersions and solvents separately. The scattering intensities at various angles (30 ~ 155°) were recorded. The scattering intensity of SWNTs was obtained by subtracting the scattering intensity of solvent from scattering intensity of dispersion.

$$I_{SWNTs} = I_{dispersion} - I_{solvent}$$

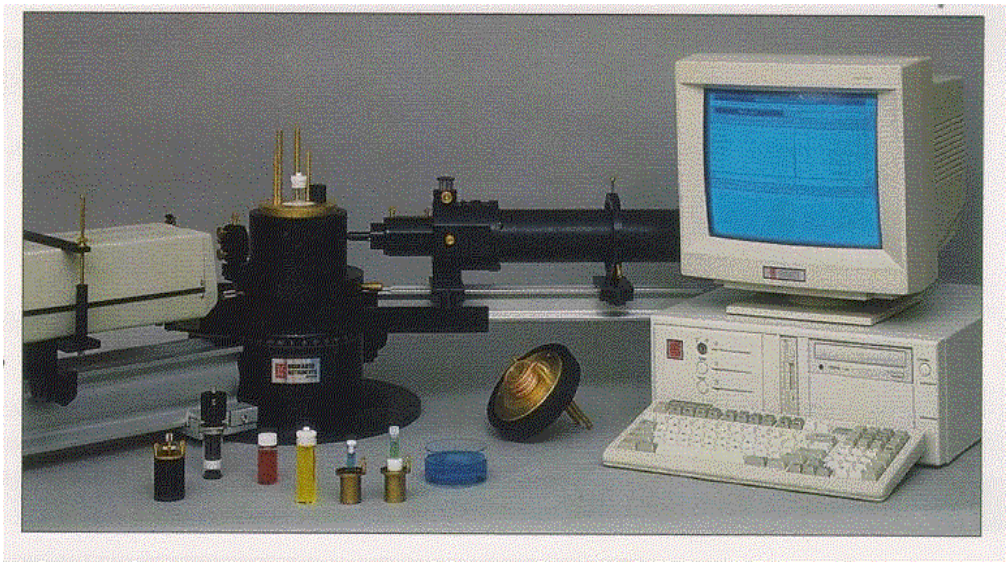

Figure 3.1 Light scattering instrument.

3.3.2 Electron Microscopy

SWNT (HiPCo) powder were observed by LEO 1530 thermally assisted FEG Scanning Electron Microscope (SEM). PVP wrapped SWNTs dispersion was observed by JEOL 4000EX high resolution TEM at 400 kV.

3.4 Light scattering model for long, thin cylinders

3.4.1 General Stokes – Mueller formalism

Stokes - Mueller formalism is a universal formalism in electromagnetic wave respectively. The basic equation is given as follows:[40]

$$S_s = M\, S_0$$

$$\begin{bmatrix} I_s \\ Q_s \\ U_s \\ V_s \end{bmatrix} = M \begin{bmatrix} I_0 \\ Q_0 \\ U_0 \\ V_0 \end{bmatrix}$$

S is stokes vector, the subscript s and 0 indicate scattered beam and incident beam. It has four components (I, Q, U, V):

I describes the total light intensity;
Q describes the amount of linear polarization along the x-axis of the (chosen) coordinate system, $Q = I_x - I_y$;
U describes the amount of linear polarization along the 45º direction of the (chosen) coordinate system, $U = I_{45^\circ} - I_{135^\circ}$;
V describes the amount of circular polarized light.

Depending on the polarization state of light, S has different forms shown in Table 3.1[41]. M is Mueller matrix, which is a 4×4 matrix. It contains all polarizing properties of the samples of randomly oriented particles, and plays an important role in light transfer processes. Every optical system can be described in terms of Mueller matrix that

transforms an input Stokes vector (I_0, Q_0, U_0, V_0) to an output Stokes vector (I_s, Q_s, U_s, V_s). The transformation process is described in Figure 3.2.

Stokes – Mueller formalism can also be written in the expanded forms.[39] For a vertically polarized incident beam, Stokes - Mueller formalism is expressed as:

$$\begin{bmatrix} Is \\ Qs \\ Us \\ Vs \end{bmatrix} = \frac{1}{k^2 r^2} \begin{bmatrix} M_{11} & M_{12} & M_{13} & M_{14} \\ M_{21} & M_{22} & M_{23} & M_{24} \\ M_{31} & M_{32} & M_{33} & M_{34} \\ M_{41} & M_{42} & M_{43} & M_{44} \end{bmatrix} \begin{bmatrix} I_0 \\ -I_0 \\ 0 \\ 0 \end{bmatrix}$$

k: wave number , $k = 2\pi/\lambda$, λ is wavelength;

r: the distance between detector and scatter.

The scattering intensity I_s, which is the first element in Stokes vector, is equal to $I_0[M_{11} - M_{12}]/k^2r^2$.

For a horizontally polarized incident beam, Stokes - Mueller formalism is expressed as:

$$\begin{bmatrix} Is \\ Qs \\ Us \\ Vs \end{bmatrix} = \frac{1}{k^2 r^2} \begin{bmatrix} M_{11} & M_{12} & M_{13} & M_{14} \\ M_{21} & M_{22} & M_{23} & M_{24} \\ M_{31} & M_{32} & M_{33} & M_{34} \\ M_{41} & M_{42} & M_{43} & M_{44} \end{bmatrix} \begin{bmatrix} I_0 \\ I_0 \\ 0 \\ 0 \end{bmatrix}$$

Scattering intensity I_s is equal to $I_0[M_{11} + M_{12}]/k^2r^2$.

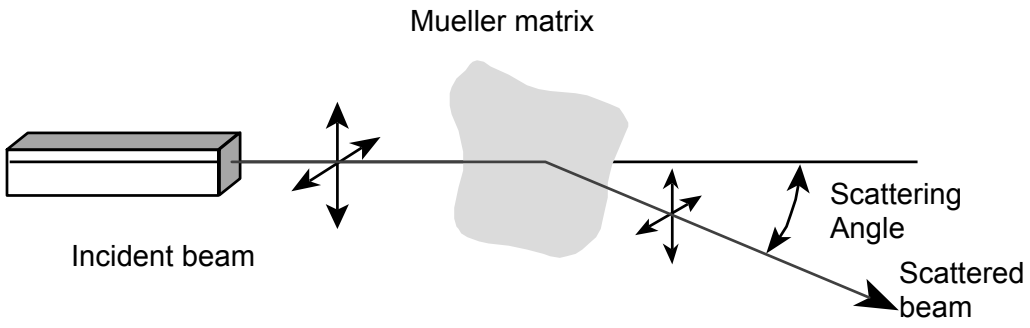

Figure 3.2 Transformation of incident beam to scattered beam by Mueller matrix

Table 3.1 Stokes vector for different polarization state of light[41]

Polarization	Stokes vector
Unpolarized light	$\begin{bmatrix} I \\ Q \\ U \\ V \end{bmatrix} = \begin{bmatrix} I \\ 0 \\ 0 \\ 0 \end{bmatrix}$
Vertically polarized	$\begin{bmatrix} I \\ Q \\ U \\ V \end{bmatrix} = \begin{bmatrix} I \\ -I \\ 0 \\ 0 \end{bmatrix}$
Horizontally polarized	$\begin{bmatrix} I \\ Q \\ U \\ V \end{bmatrix} = \begin{bmatrix} I \\ I \\ 0 \\ 0 \end{bmatrix}$

3.4.2 Stokes - Mueller formalism for long, thin cylinders

Mueller matrix depends on different scattering systems. SWNT is a long, thin cylindrical structure. To apply Stokes – Mueller formalism to SWNT, a Mueller matrix for long, thin cylinder is required. Yaoming Shi and M. McClain proposed a closed form of Mueller scattering matrix for a random ensemble of long, thin cylinders.[42] These cylinders may be transparent or absorbing. The cylinder radius a and length L must obey $a < \lambda_{med}/2\pi < L$. SWNTs with diameter of several nm and length of several μm can satisfy these conditions. In McClain model, all 16 elements in Mueller matrix were calculated. However, not all of them are needed here. Since the detector of light scattering instrument measures scattering intensity I_s, which is the first element in Stokes vector, only the first row of Mueller matrix is what we are concerned with.

Furthermore, when the incident beam is either vertically or horizontally polarized, only M_{11} and M_{12} are needed.

When $I_s(\theta)$ is normalized to a certain angle θ^*, the incident intensity I_0, k and r will be canceled out. Thus the final form can be simplified as follows:

For vertically polarized incident beam, I_s at any angle θ is normalized to that at a specific angle θ^* as:

$$I_S(\theta) / I_S(\theta^*) = [M_{11}(\theta) - M_{12}(\theta)] / [M_{11}(\theta^*) - M_{12}(\theta^*)]$$

For a horizontally polarized incident beam, I_s at any angle θ is normalized to that at a specific angle θ^* as:

$$I_S(\theta) / I_S(\theta^*) = [M_{11}(\theta) + M_{12}(\theta)] / [M_{11}(\theta^*) + M_{12}(\theta^*)]$$

In McClain model, M_{11} and M_{12} are found to be:

$$M_{11}(\theta) = |\mu|^2 \sum_{n=0}^{3} a_n^{11} (5-n)! \mathrm{Re}\left[{}_2F_2(1,1:2,6-n;2ikL|\sin 0.5\theta|\right]$$

$$M_{12}(\theta) = |\mu|^2 \sum_{n=0}^{3} a_n^{12} (5-n)! \mathrm{Re}\left[{}_2F_2(1,1:2,6-n;2ikL|\sin 0.5\theta|\right]$$

	M_{11}	M_{12}
n	$(5-n)!\ a_n^{11}$	$(5-n)!\ a_n^{12}$
0	$-(m'^2-1)^2(19-10c+3c^2)$	$(m'^2-1)^2(1+c)(7+3c)$
1	$(m'^2-1)^2(19-10c+3c^2)$	$-(m'^2-1)^2(1+c)(7+3c)$
2	$-2(m'^2-1)[-9+10c+3c^2+(1+c)^2m'^2]$	$2(1+c)(m'^2-1)[5+3c+(3+c)\,m'^2]$
3	$[(17-6c+9c^2)+(-2+4c+6c^2)\,m'^2+(1+c)^2m'^4]$	$-(1+c)(m'^2+3)[-5+3c+(1+c)m'^2]$

c = cosθ;

k: $k = 2\pi n_{medium} / \lambda_{vac}$;

m: relative refractive index, $m = (n+K^*i)_{cylinder}/n_{medium} = m' + m''\,I$;

K: extinction coefficient;

m': real part of relative refractive index;

L: length of cylinder; a: radius of cylinder;

$\mu = a^2L(m^2-1)/4(m^2+1)$.

In which, ${}_2F_2$ is hypergeometric function. It is defined as:[43]

$${}_2F_2(a_1,a_2;b_1,b_2;z) = \sum_{k=0}^{\infty} \frac{(a_1)_k (a_2)_k z^k}{(b_1)_k (b_2)_k k!}$$

Input $M_{11}(\theta)$ and $M_{12}(\theta)$ expressions into normalized $I_S(\theta)$ equation, the following equation can be obtained:

For vertically polarized incident beam:

$$I_S(\theta) / I_S(\theta^*) = [M_{11}(\theta) - M_{12}(\theta)] / [M_{11}(\theta^*) - M_{12}(\theta^*)]$$

$$= \frac{\sum_{n=0}^{3} a_n^{11}(5-n)!\,\mathrm{Re}\left[{}_2F_2(1,1:2,6-n;2ikL\left|\sin 0.5\theta\right|\right] - \sum_{n=0}^{3} a_n^{12}(5-n)!\,\mathrm{Re}\left[{}_2F_2(1,1:2,6-n;2ikL\left|\sin 0.5\theta\right|\right]}{\sum_{n=0}^{3} a_n^{11}(5-n)!\,\mathrm{Re}\left[{}_2F_2(1,1:2,6-n;2ikL\left|\sin 0.5\theta^*\right|\right] - \sum_{n=0}^{3} a_n^{12}(5-n)!\,\mathrm{Re}\left[{}_2F_2(1,1:2,6-n;2ikL\left|\sin 0.5\theta^*\right|\right]}$$

For horizontally polarized incident beam:

$$I_S(\theta) / I_S(\theta^*) = [M_{11}(\theta) + M_{12}(\theta)] / [M_{11}(\theta^*) + M_{12}(\theta^*)]$$

$$= \frac{\sum_{n=0}^{3} a_n^{11}(5-n)!\,\mathrm{Re}\left[{}_2F_2(1,1:2,6-n;2ikL\left|\sin 0.5\theta\right|\right] + \sum_{n=0}^{3} a_n^{12}(5-n)!\,\mathrm{Re}\left[{}_2F_2(1,1:2,6-n;2ikL\left|\sin 0.5\theta\right|\right]}{\sum_{n=0}^{3} a_n^{11}(5-n)!\,\mathrm{Re}\left[{}_2F_2(1,1:2,6-n;2ikL\left|\sin 0.5\theta^*\right|\right] + \sum_{n=0}^{3} a_n^{12}(5-n)!\,\mathrm{Re}\left[{}_2F_2(1,1:2,6-n;2ikL\left|\sin 0.5\theta^*\right|\right]}$$

In above equations, the effects of extinction coefficient and radius of cylinders are cancelled out by normalization.

Refractive index of SWNT n is taken the value of graphite, which is 2.5.[44] The refractive index of water and oleum is 1.33 and 1.83. There is difference of refractive index between SWNTs and solvent, which would cause scattering as light passes through the dispersion. At a given angle, input assumed extinction coefficient K and radius a of SWNTs, a curve of the normalized scattering intensity for a single SWNT with various lengths can be plotted as a function of wave vector q ($q = 4\pi\sin(\theta/2)/\lambda$). On the other hand, a plot of normalized I_s as a function of q can be obtained from experiments. Comparing the simulated curve with experimental curve, the average SWNT length can be determined.

The only assumptions made in using McClain model is that there is no multiple scattering in SWNT dispersion, which can make the experimental result comparable to the simulated result. In experiment, what has been measured is the total scattering intensity of SWNTs. However, the Stokes - Mueller formalism is used for a single particle. If there is only single scattering in SWNT dispersion, the total scattering intensity can be taken as the summation of scattering intensity of individual tube or bundles. Thus it is possible to correlate experimental results to simulated results.

CHAPTER 4

RESULTS AND DISCUSSIONS

4.1 Morphology of SWNTs

4.1.1 Morphology of SWNT powder

SWNTs tend to form entangled network in solid state. Figure 4.1 is SEM of SWNT powder (HiPCo). Most of tubes form bundles, which have diameters of about 35 nm.

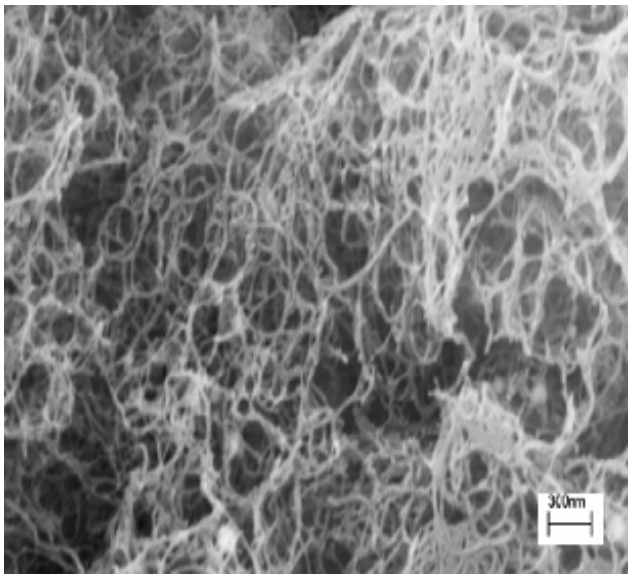

Figure 4.1 SEM of SWNT powder (HiPCo).

4.1.2 Morphology of PVP wrapped SWNT dispersion

Individual SWNT can be obtained in polyvinyl pyrrolidone (PVP) wrapped SWNTs aqueous dispersion. With the aid of Sodium Dodecyl Sulfate (SDS), the strong interaction between SWNTs is disrupted, and PVP wrapped around SWNTs, and form a homogenous dispersion. There is no particle that can be seen under optical microscopy.

(Figure 4.2). AFM images give the evidence of existence of individual SWNT, which is a rigid rod covered by a monolayer of polymer (Figure4.3).[38]

Figure 4.2 Optical microscopy of PVP wrapped SWNT water dispersion.

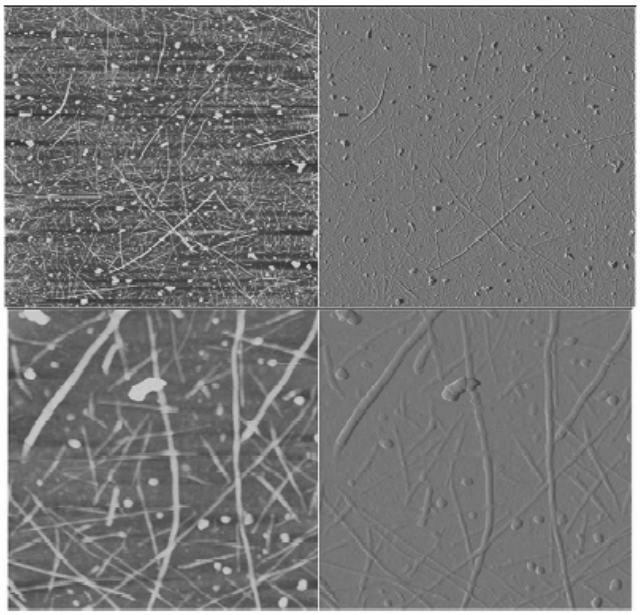

Figure 4.3 Tapping - mode AFM images of PVP wrapped SWNTs on a functionalized substrate. 5 μm height image (top left) and amplitude image (top right) 1μm expanded height image (bottom left) and amplitude image (bottom right).[38]

4.1.3 Morphology of SWNTs in oleum

An optically transparent SWNT dispersion in oleum containing 30 % SO_3 was prepared in our lab. No SWNT aggregates were observed in the dispersion (Figure 4.4). Thus the dispersion is judged to be optically uniform.

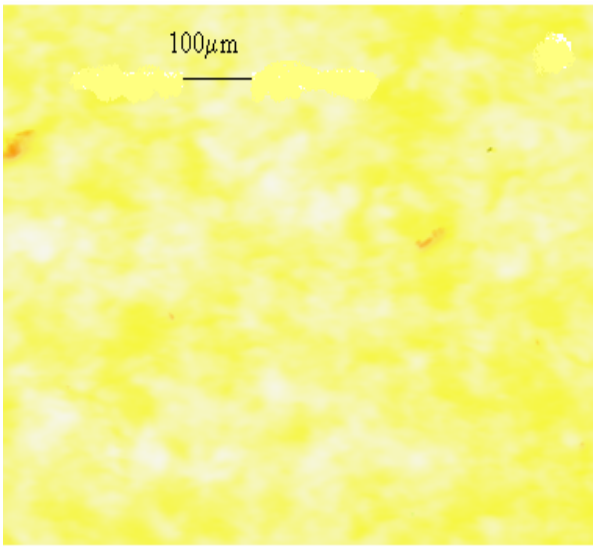

Figure 4.4 Optical microcopy of SWNT/oleum dispersion.

4.2 Optical properties of SWNTs

In Figure 4.5, absorption spectra of SWNTs are shown. The individual SWNT has shaper peaks than those of bundles. For both isolated SWNT and bundles, weak peaks occur between wavelength of 500 and 700 nm, indicating light absorbance of SWNTs in this range. The wavelength of laser beam used in this study is 633 nm, thus the light absorption of SWNTs needs to be considered in the model.

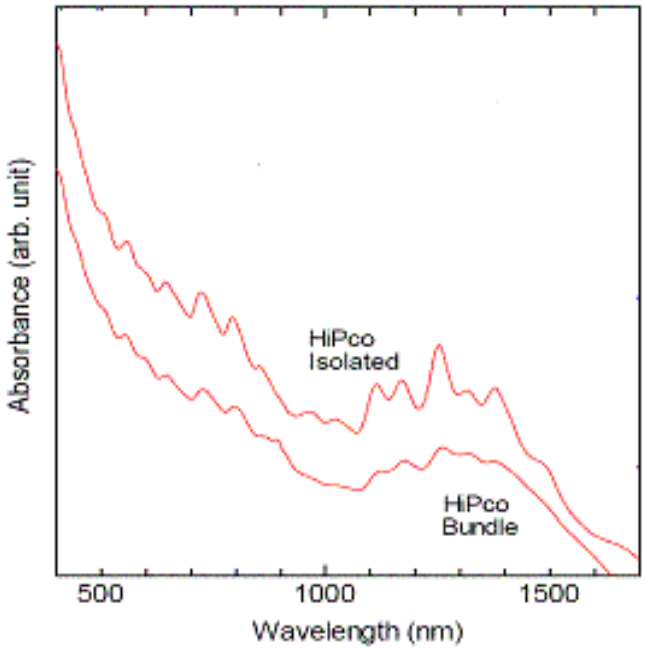

Figure 4.5 Absorption spectrum of SWNTs (both samples were sonicated and dispersed in D_2O (1% SDS), for isolated sample, the suspension was centrifuged, and its supernatant used for the exclusion of bundled SWNTs).[45]

4.3 Light scattering from SWNTs

4.3.1 Effect of filtration on solvent scattering

The scattering intensity is greatly affected by impurities. To remove impurities, filtration or centrifugation should be used. In this research, filtration was used to prepare the samples. First let us see the effect of filtration on scattering intensities of pure solvents (water and oleum). Their scattering intensities before and after filtration were plotted as a function of wave vector q in Figures 4.6 ~ 4.7. It can be seen that filtration is an effective way to remove the impurities in water. After filtration, the scattering intensity of water became uniform at different angles. However, high scattering intensities of oleum still occur at small angles. This is because of oxidation of filter by oleum, which may bring some new impurities to the dispersion. Therefore, studies on SWNT/oleum dispersion were conducted without filtration. Meanwhile, filtration was also not used on

PVP wrapped SWNT and SWNT/oleum stock dispersions. The diameter of filter pore is 200 nm, and would block most of SWNTs passing through. To avoid the removal of

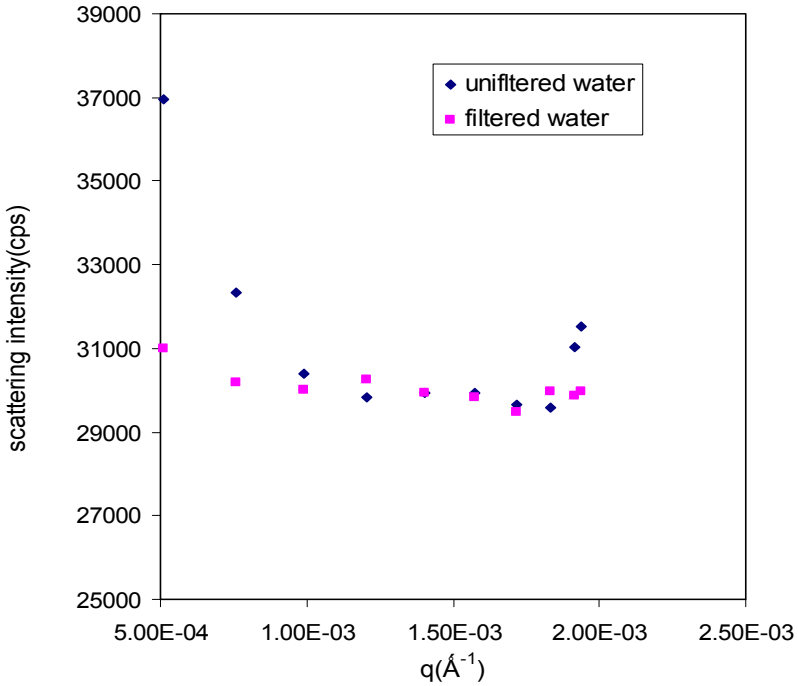

Figure 4.6 Effect of filtration on scattering intensity of water.

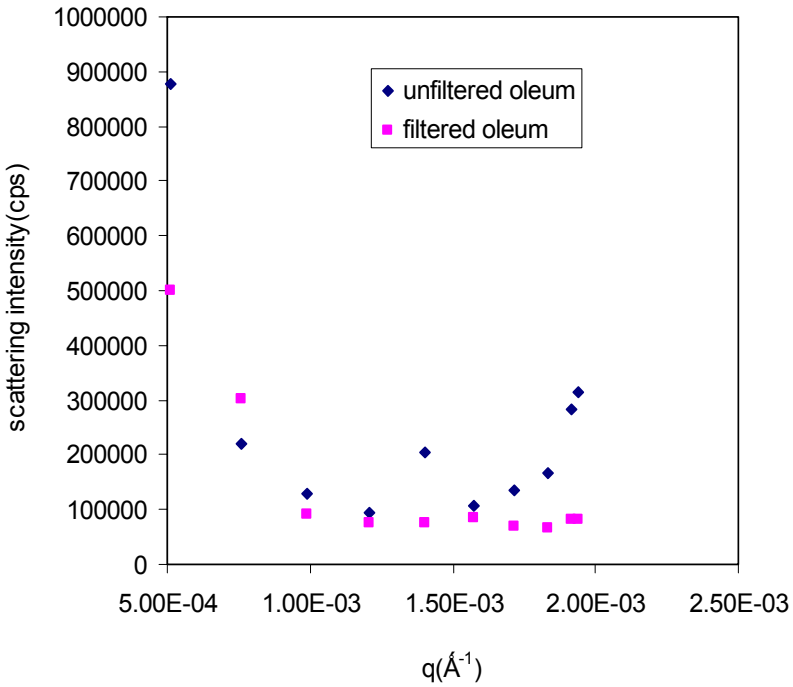

Figure 4.7 Effect of filtration on scattering intensity of oleum.

SWNTs, the unfiltered SWNT water and oleum dispersions were used.

4.3.2 Single scattering

Scattering intensity obtained from Stokes- Mueller formalism is for single particle, while the scattering intensity measured experimentally is for the total number of particles. To make these two results comparable, SWNT in the dispersion must be single scattering, which means that the scattering of SWNT would not interfere with each other, scattering intensity is additive. If there are M particles in the solution, the total scattering intensity is M times that scattered by a single particle, and the energy removed from the original beam is also M times that removed by a single particle.[46] It is called as single scattering in this case. When the scattering of particles interfere with each other, the scattering intensity is no longer additive, multiple scattering occurs. Single scattering can be determined by observing the change of scattering intensity with concentration. In Figure 4.8 and 4.9, the scattering intensities of PVP wrapped SWNT and SWNT/oleum dispersions were plotted as a function of concentration. It can be seen that the scattering intensity almost linearly scales with concentration for both of dispersions, thus, the assumption of single scattering in PVP wrapped SWNT and SWNT/oluem has been verified.

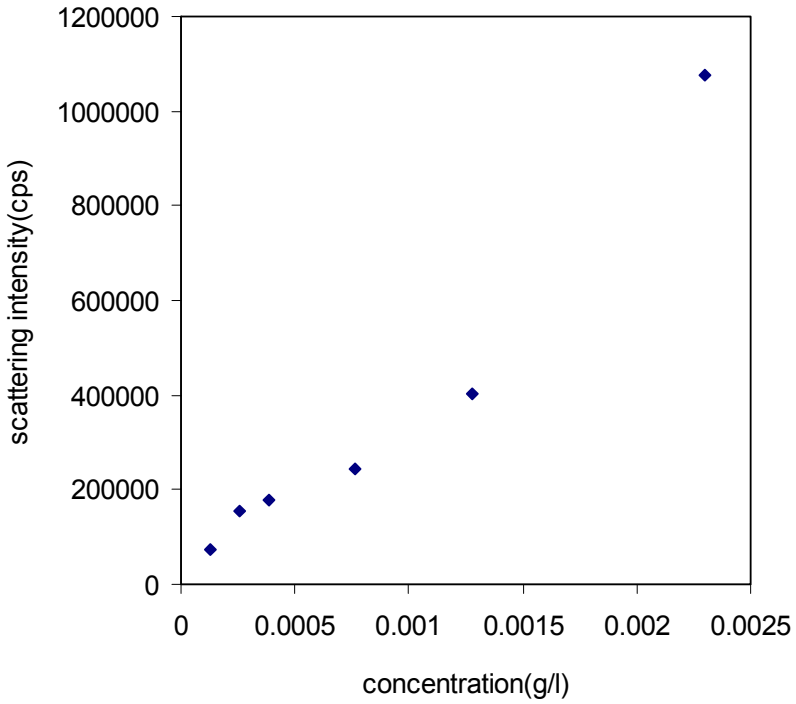

Figure 4.8 Scattering intensity as a function of concentration for PVP wrapped SWNT dispersion (at 60°).

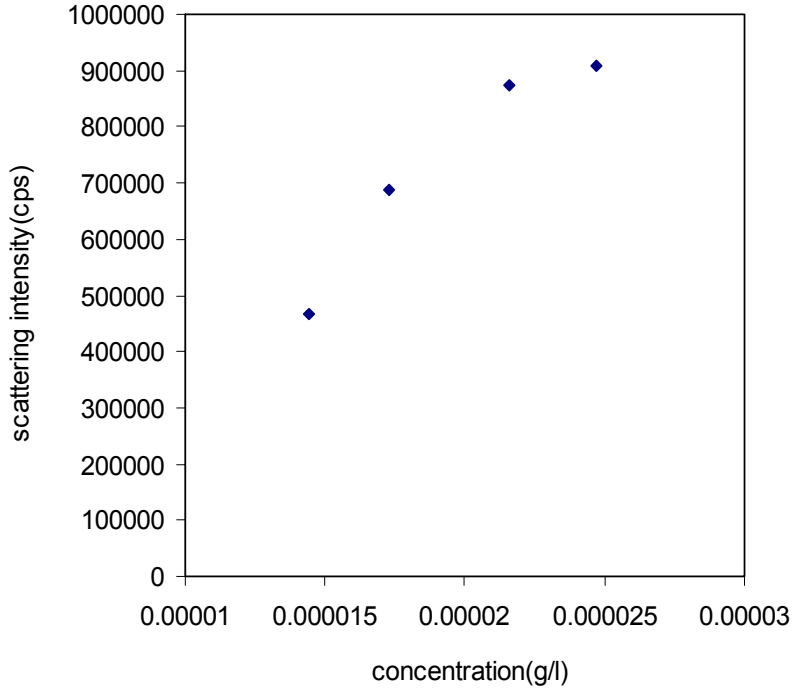

Figure 4.9 Scattering intensity as a function of concentration for SWNT/oleum dispersion (at 60°).

4.3.3 Scatting curves of SWNTs predicted by McClain model

In Stokes – Mueller formalism for vertically or horizontally polarized incident beam, the element of M_{11} and M_{12} are needed for determining the scattering intensity. In McClain model for long, thin cylinders, M_{11} and M_{12} can be calculated if refractive index, extinction coefficient, radius and length of SWNTs are known. Refractive index of SWNT has not been reported, it is approximately taken as 2.5, which is the value of graphite. Therefore, the effect of other factors will be studied, and scattering curves will be plotted.

1. Predicted scattering curves of SWNTs with varying extinction coefficients or radii

   For a given length and radius, normalized scattering intensity of SWNTs with varying extinction coefficients will be plotted as a function of wave vector q. For a given length and extinction coefficient, normalized scattering intensity of SWNTs with varying radii will be plotted as a function of q (for vertically polarized and horizontally polarized incident beam).

2. Predicted scattering curves of SWNTs shot by laser beams with different wavelengths

   For a SWNT with given length, radius and extinction coefficient, normalized scattering intensity of SWNTs shot by laser beam with different wavelengths will be plotted as a function of wave vector (for vertically polarized and horizontally polarized incident beam).

3. Determination of SWNT length

   For a given radius and extinction coefficient, normalized scattering intensity SWNTs with varying lengths will be plotted as a function of wave vector (for vertically polarized and horizontally polarized incident beam). The length of SWNTs will be determined by comparing the simulated curves with experimental curves.

4.3.3.1 Predicted scattering curves of SWNTs with varying extinction coefficients or radii

For light absorbing particles, the refractive index has a complex form with the imaginary part (extinction coefficient) indicating the absorption. The real part of refractive index of SWNTs is assumed to be the same as that of graphite, which is 2.5. At a given angle, assuming SWNTs with 1 nm diameter and length of 1 μm, and input by various extinction coefficients (0.1, 0.3, 0.6, 1.0), M_{11} and M_{12} were calculated. In the same way, assuming that SWNT length is 1μm and extinction coefficient is 0.3, M_{11} and M_{12} were calculated for various tube radii (0.5, 1, 1.5, 2 nm). Then, scattering intensity at scattering angle θ is normalized to that at 30˚, which is expressed in the following equation(for vertically polarized beam)

$I_s(\theta) / I_s(30°) = ([M_{11}(\theta) - M_{12}(\theta)]I_0 / k^2r^2) / ([M_{11}(30°) - M_{12}(30°)] I_0 / k^2r^2)$

$$= \frac{\sum_{n=0}^{3} a_n^{11}(5-n)!\,\mathrm{Re}\left[{}_2F_2(1,1:2,6-n;2ikL\left|\sin 0.5\theta\right|\right] - \sum_{n=0}^{3} a_n^{12}(5-n)!\,\mathrm{Re}\left[{}_2F_2(1,1:2,6-n;2ikL\left|\sin 0.5\theta\right|\right]}{\sum_{n=0}^{3} a_n^{11}(5-n)!\,\mathrm{Re}\left[{}_2F_2(1,1:2,6-n;2ikL\left|\sin 0.5*30\right|\right] - \sum_{n=0}^{3} a_n^{12}(5-n)!\,\mathrm{Re}\left[{}_2F_2(1,1:2,6-n;2ikL\left|\sin 0.5*30\right|\right]}$$

Both the extinction coefficient and the SWNT radius are cancelled out by normalization. The plots for PVP wrapped SWNT and SWNT/oleum dispersions for various extinction coefficients or radii are shown in Figure 4.10 and 4.11, all of which fall onto a single curve. The advantage of normalization is that length effect can be investigated independently.

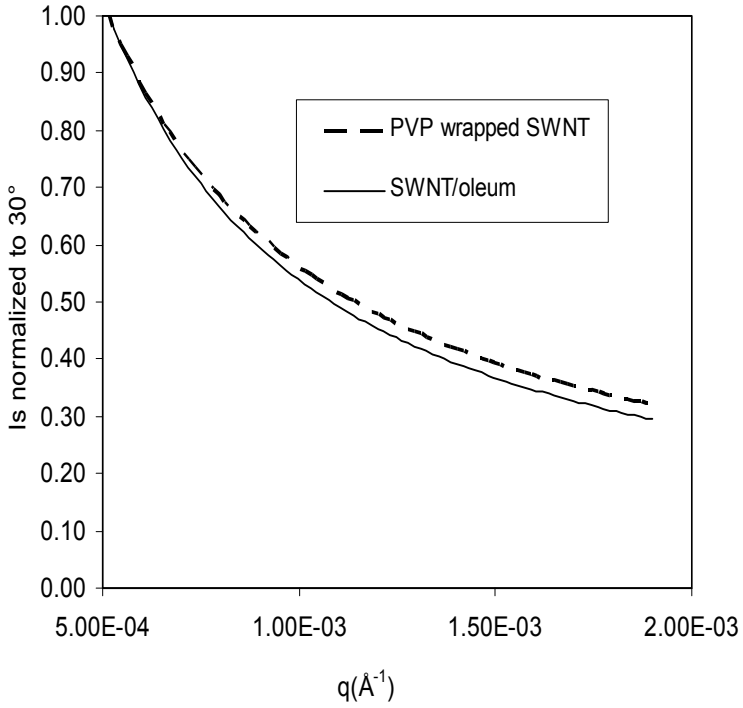

Figure 4.10 Normalized scattering intensity as function of wave vector for SWNT with various extinction coefficients and radii (vertically polarized beam. Length of SWNT is assumed to be1 μm, refractive index is 2.5).

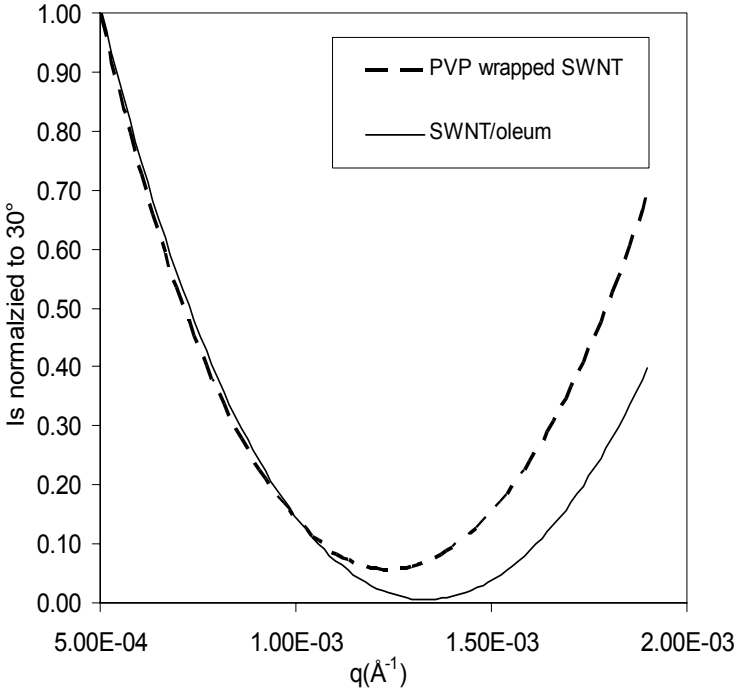

Figure 4.11 Normalized scattering intensity as a function of wave vector for SWNT with various extinction coefficients and radii (horizontally polarized beam. Length of SWNT is assumed to be1 μm, refractive index is 2.5).

4.3.3.2 Predicted scattering behavior of SWNTs for different laser wavelengths

The effect of wavelength of incident beam on scattering behavior of SWNTs was

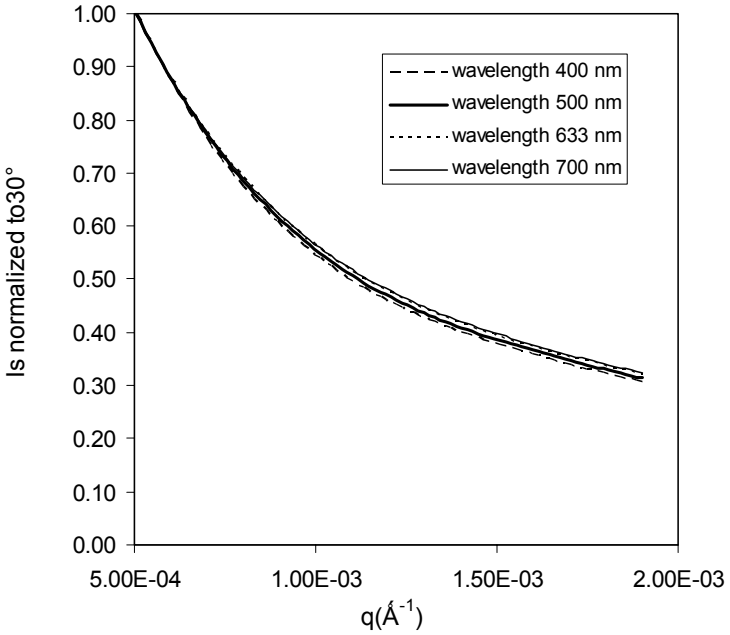

Figure 4.12 Scattering curves of SWNT for various laser wavelengths (vertically polarized incident beam, length of SWNT is assumed to be 1 μm, refractive index is 2.5).

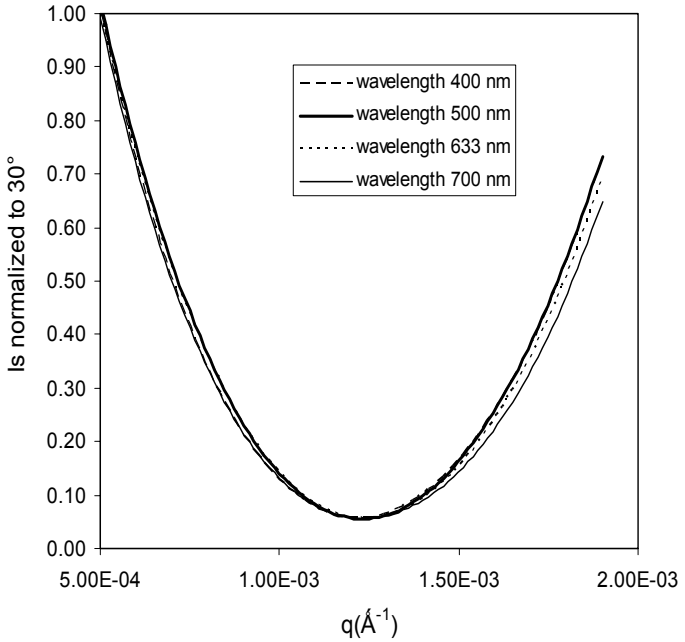

Figure 4.13 Scattering curves of SWNT for various laser wavelengths (horizontally polarized incident beam, length of SWNT is assumed to be 1μm, refractive index is 2.5).

predicted. The normalized scattering intensities of SWNTs for various wavelengths of incident beam were plotted as a function of wave vector in Figures 4.12 ~ 4.13. It can be seen that the curves almost overlap for different wavelengths.

4.3.3.3 Determination of SWNT length

Both radius and extinction coefficients of SWNT have no effect on normalized scattering intensity curves, which indicate that the average length of SWNTs can be determined without consideration of these two factors. Normalized scattering intensities of PVP wrapped SWNTs and SWNT/oleum with SWNTs of various lengths were simulated as a function of wave vector, and the plots are given in Figures 4.14 ~ 4.17. The experimental curves are also plotted. It was found that in PVP wrapped SWNT aqueous dispersion, the simulated curve corresponding to 600 nm long SWNT best fits with the experimental curve. However, in SWNT/oleum dispersion, the simulated curve did not fit well with experimental data. The reason will be discussed in the following section. In Figure 4.15, it can be seen that the normalized scattering intensity for long length (> 1μm) almost overlap. This is because of the length scale that is used for measurement (1000 nm ~ 100 nm). The instrument could not tell the difference once the length of particle is beyond 1 μm.

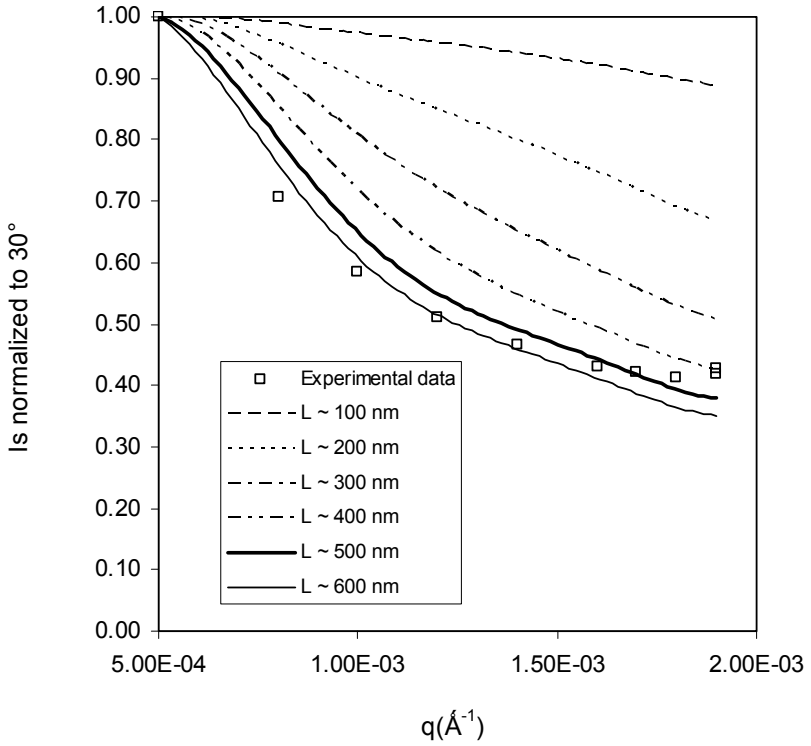

Figure 4.14 Length effect of SWNTs on scattering curves for vertically polarized incident beam (PVP wrapped SWNTs aqueous dispersion, refractive index of SWNT is 2.5).

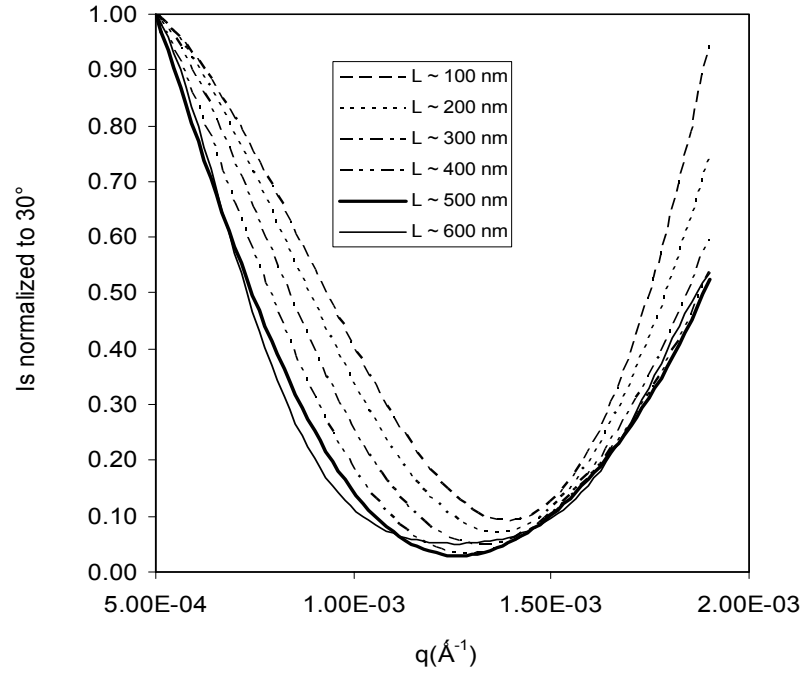

Figure 4.15 Length effect of SWNTs on scattering curves for horizontally polarized incident beam (PVP wrapped SWNTs aqueous dispersion, refractive index of SWNT is 2.5).

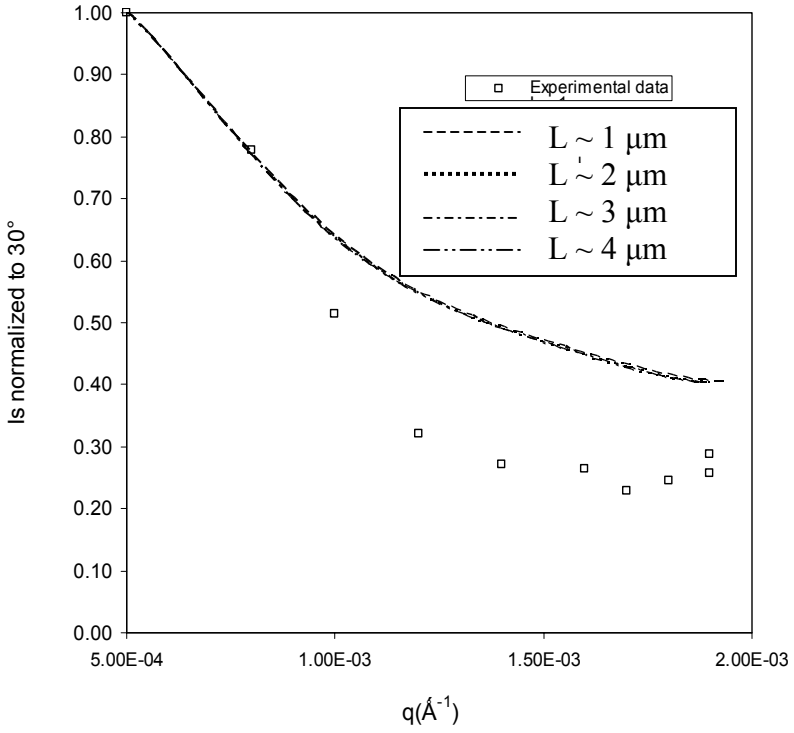

Figure 4.16 Length effect of SWNTs on scattering curves for vertically polarized incident beam (SWNTs in oleum, refractive index of SWNT is 2.5).

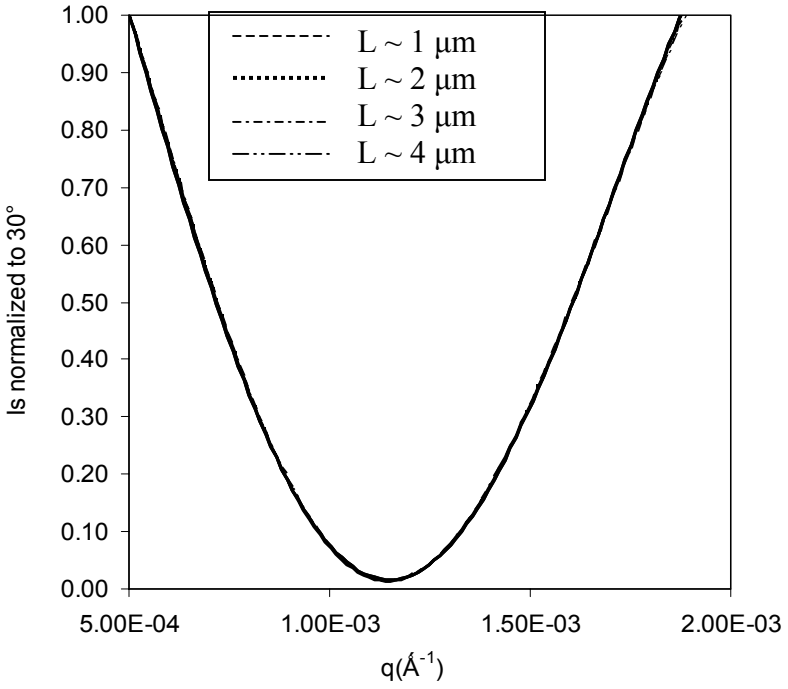

Figure 4.17 Length effect of SWNTs on scattering curves for horizontally polarized incident beam (SWNTs in oleum, refractive index of SWNT is 2.5).

4.3.3.3 Discussions

The experimental curves for either PVP wrapped SWNTs aqueous or SWNT oleum dispersion do not perfectly fit with simulated curves. The reason may be attributed to the impurities in the samples. In PVP wrapped SWNTs aqueous dispersion, the impurities in water can be removed by filtration. However, some impurities may still remain. Transmission electron microscopy images give the evidence of the existence of iron and amorphous carbon particles (presence of iron particles is shown by arrows), which would affect the scattering intensity (Figures 4.18 ~ 4.19). In SWNT oleum dispersion, no filtration was conducted on either oleum or stock solution, impurities can come from both oleum and SWNTs, which affect results greatly.

The other reason may come from the morphology of SWNTs in dispersions. It is assumed that SWNTs behave as rigid rod structure in both of these dispersions. Therefore, Mueller matrix proposed by McClain et al. for long, thin cylindrical structures was used. However, there might be entangled network existing in the dispersion. To investigate the morphology of SWNTs in dispersion, fractal dimension was determined by plotting $\ln(I_s)$ as a function of $\ln(q)$ (Figure 4.20 ~ 21). The fractal dimension can be determined by the slope of the fitted line. If SWNTs exist as rigid rod structure, the fractal dimension would be 1. However, fractal dimensions for both the dispersions are non integer value, and are between 1 and 2, indicating that the morphology of SWNTs in these two dispersions is between rigid rod and entangled network. Specifically, for SWNT/oluem dispersion, no sonication was conducted, and longer tubes exist, which easily form entangled network. As long as network form, the Mueller matrix, which describes rigid rod structure, will not be applicable.

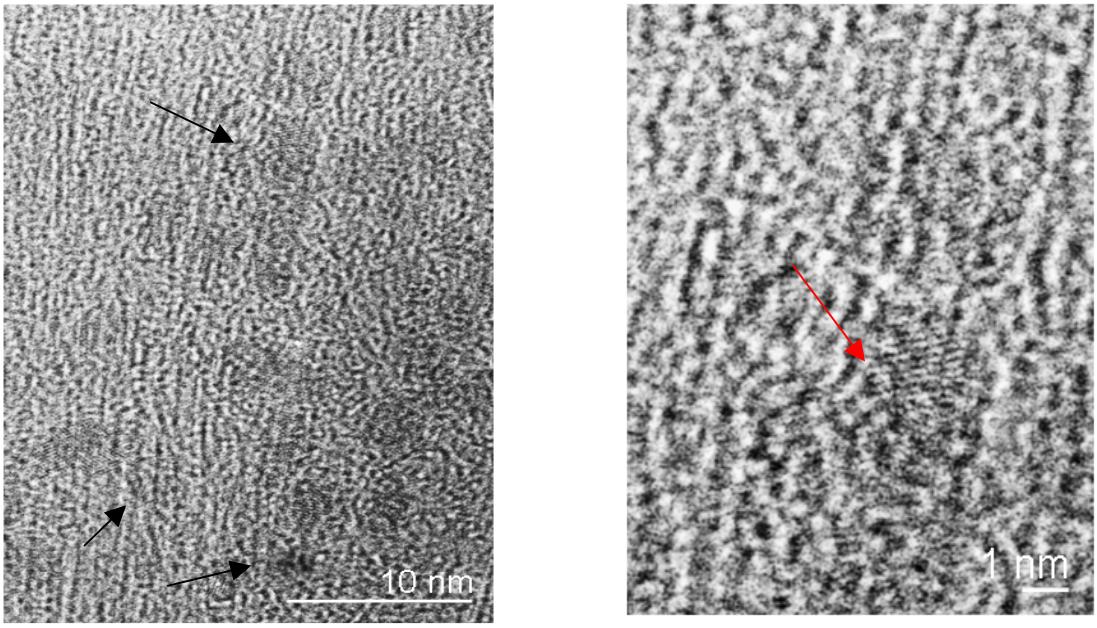

Figure 4.18 Transmission electron microscopy of PVP wrapped SWNT aqueous dispersion (iron particles).

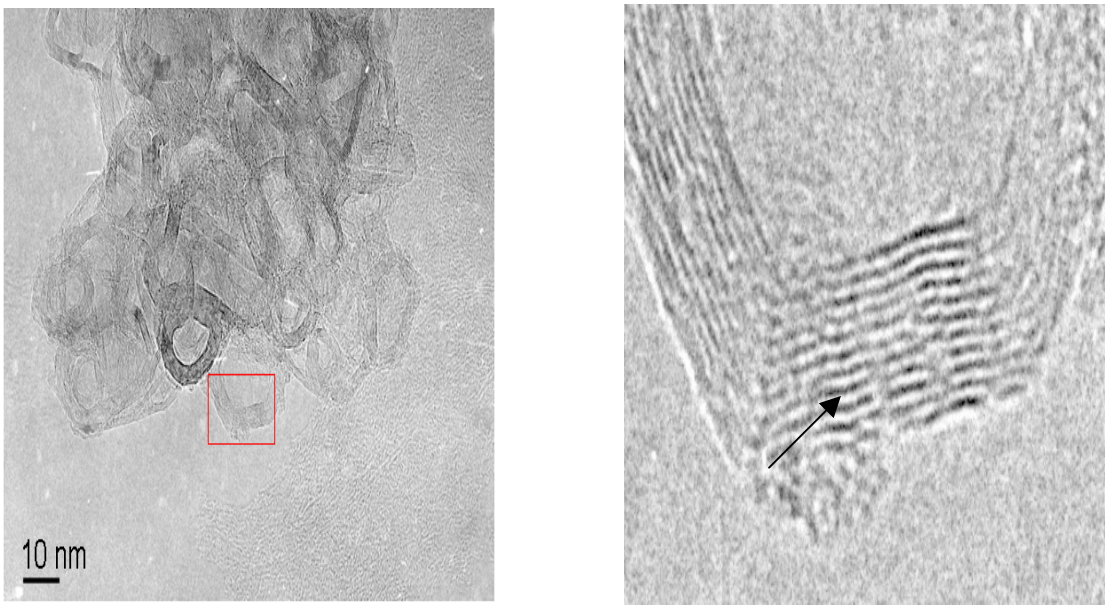

Figure 4.19 Transmission electron microscopy of PVP wrapped SWNT aqueous dispersion (amorphous carbon).

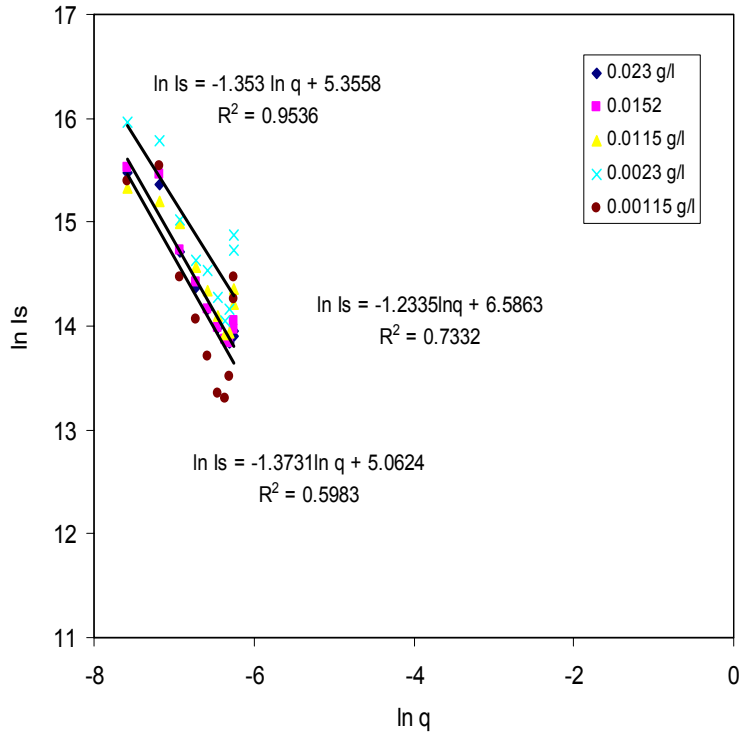

Figure 4.20. Fractal dimension of PVP wrapped SWNT water dispersion

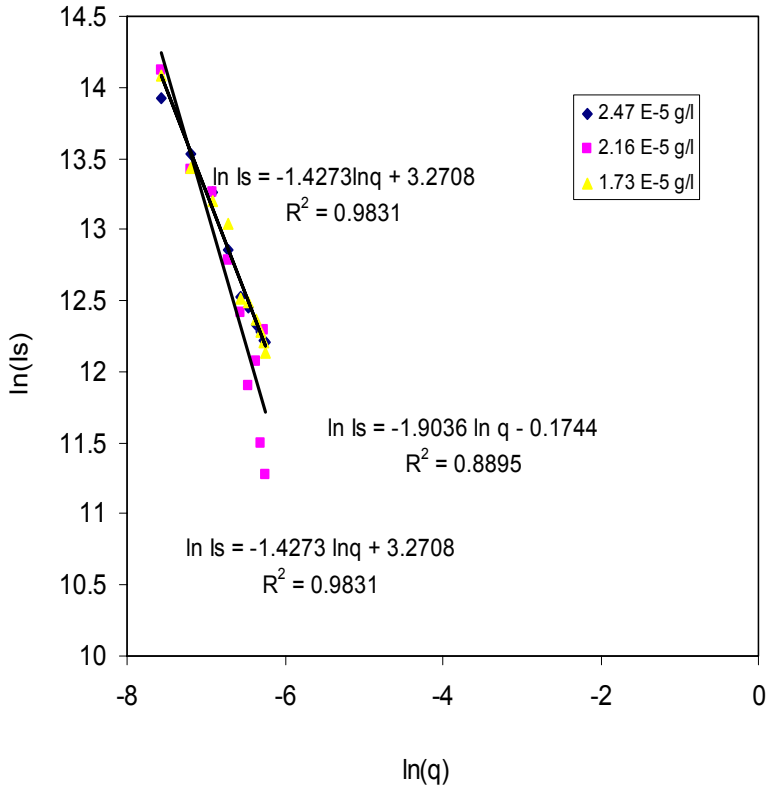

Figure 4.21 Fractal dimension of SWNT in oleum

4.4 Molecular weight of SWNTs

4.4.1 Theoretical calculation of molecular weight of SWNT from atomic structure

Molecular weight of SWNT can be calculated based on its atomic structure. On the graphite sheet (Figure 2.3), a unit cell of carbon nanotube is defined, which is the rectangle bounded by the vectors $\vec{C}_h$ and $\vec{T}$, where $\vec{T}$ is the1D translation vector of the nanotube. The vector $\vec{T}$ is normal to $\vec{C}_h$ and extends from the origin to the first lattice point B in the honeycomb lattice. The number of carbon atoms per unit cell of the 1D tubule n_c can be calculated by the following equation:

$$n_c = 4(n^2+m^2+nm)/d_R$$

d_R is the highest common divisor of (2n+m, 2m+n)

Length of $\vec{T}$ is given as:

$$|T| = \sqrt{3}L/d_R$$

L: circumference of nanotube, $L = |C_h| = a(n^2 + m^2 + nm)$;

a: length of unit vector, $a = \sqrt{3}a_{C-C}$;

a_{c-c} :carbon-carbon bond, a_{c-c} = 1.42 Å.

For an individual tube of length L_t, the total number of carbon atoms N is:

$$N = L_t n_c/|T|$$

$$MW = \frac{\mathbf{48}\pi Ltd}{\mathbf{3}\sqrt{\mathbf{3}}a_{c-c}^{\mathbf{2}}}$$

Based on this equation, molecular weight of an individual SWNT can be calculated if the diameter and length are known. In PVP wrapped SWNT dispersion, length of SWNT is 600 nm and diameter is about 1.2 nm, [38] therefore, MW is 1.04 E+6 g/mol.

4.4.2 Zimm plot

In static light scattering, Zimm plot is generally used to determine the molecular weight and size of particles. The formula of Zimm plot is written as follow:[47]

$$H\, c/\Delta R(\theta.\, c) = (1/ M_w)\, [1+(R_g^2 q^2)/3] + 2A_2 c$$

H: an instrumental constant, $H = 4\pi^2 n_0^2 (dn/dc)^2/(N_0 \lambda_0^4)$;

n_0: refractive index of the solvent; dn/dc: specific refractive index increment of the solution;

N_0: Avogadro's number; λ_0: laser wavelength in vacuum of the laser;

c: solution concentration;

θ: scattering angle;

Δ R: excess Rayleigh ratio. $\Delta R = R_{soln} - R_{solv}$;

M_w: weight average molecular weight;

A_2: the second viral coefficient;

q : the magnitude of the scattering wave vector, $q = (4\, \pi n_0/ \lambda_0)\sin(\theta/2)$;

R_g; particle radius of gyration.

The scattering intensities at different angles and different concentrations can be measured. If the left side of equation is plotted against $\sin^2 (\theta/2) + kc$, where k is a constant, a grid like plot results. One set consists of angular measurement at each concentration, and one set consists of concentration measurements at each angle. Extrapolating the angular measurements to zero angle for each concentration yields a straight line in c. The slope of this line yields A_2. Extrapolating the concentration measurements to zero concentration for each angle yields a straight line in $\sin^2 (\theta/2)$. The slope divided by the intercept of this line yields R_g. The intercept of both extrapolated lines yields molecular weight.

Zimm plot has been widely used in determining the molecular weight, gyration radius and second viral coefficient of polymers.[4849] However, light scattering can not determine the molecular weight of SWNTs since it can not tell the individual tube from tube bundles. Assume there are two SWNTs dispersions, one has individual tube with diameter of 1nm; another one has SWNT bundles with diameter of 10 nm. The lengths

of SWNTs in both dispersions are same. Based on the molecular weight formula derived in section 4.4.1, molecular weight of SWNT bundles in the latter dispersion would be much higher than the former one. However, we could not get the same information from light scattering. The light scattering intensity of these two dispersions would not show significant difference. To better explain this phenomenon, scattering intensity of SWNTs with different lengths was plotted as a function of diameter in Figure 4.22. Since the scattering angle is from 30 ~ 155°, the length scale used is for 100 nm to 1000 nm ($1/q_{min} < L < \pi/q_{max}$, $q = 4\pi \sin(\theta)/\lambda$). This length scale determines that light scattering instrument could not tell the difference of scattering from small SWNT bundle As the bundle size is large enough, its molecular weight can be determined by light scattering.

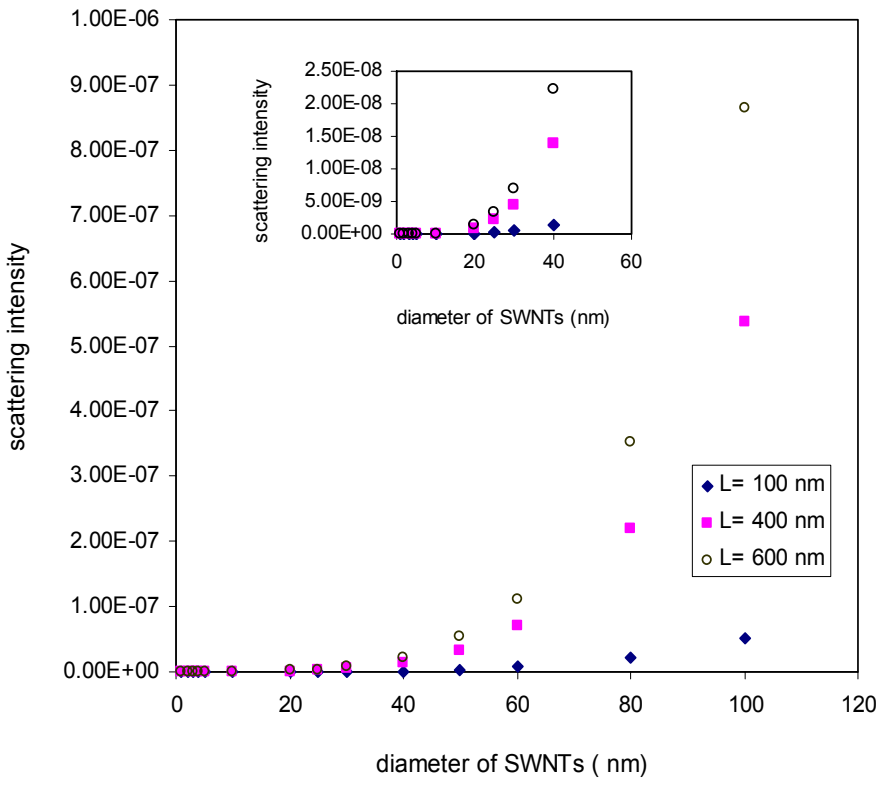

Figure 4.22 Scattering intensity as a function of bundle diameter

4.5 Effect of concentration on scattering intensity of SWNTs at a certain angle

At a certain angle, scattering intensity was determined for various concentrations of PVP wrapped SWNT aqueous dispersion. If only scattering exist, the scattering intensity would increases with increasing SWNT concentration. However, in this experiment, an interesting phenomenon was observed. At a certain angle, the scattering intensity was plotted as a function of concentration (Figure 4.23). The figure shows the existence of critical concentration (C*) of SWNT. Below C*, scattering intensity increases with concentration; above C*, scattering intensity decreases with concentration. This phenomenon happened at every measured angle. This may be attributed to light absorption of SWNTs. To verify it, a similar curve was predicted from Beer-Lambert law. Beer-Lambert law describes the attenuation of light when it passes through absorptive medium. The general Beer-Lambert law is written as:[50]

$$A = -\ln(I/I_0) = \varepsilon \ell c$$

A: the measured absorbance;
I: the light intensity after it passes through the sample;
I_o: the incident light intensity;
ε: a wavelength-dependent molar absorption coefficient (unit: l/(mol·cm));
ℓ: the path length; c: solution concentration (mol/l).

Based on Beer–lambert law, scattering intensity I_s was plotted as a function of concentration c ($I_s = I_0 e^{-\varepsilon c l}$) in Figure 4.23. It can be seen that it goes up then falls down, which is similar to experimental data. Further, molar absorption coefficient of dispersion can also be found out by Beer-Lambert law. The process of a beam of light passing through an absorptive medium is sketched in Figure 4.24. When a beam of light (I_0) passes through a light path ℓ, it is absorbed, and becomes I_1. I_1 is further scattered by a scattering volume (I_s), passes through a light path ℓ, and reaches the detector (I_2). What light scattering instrument measures is relative intensity I_2/I_0.

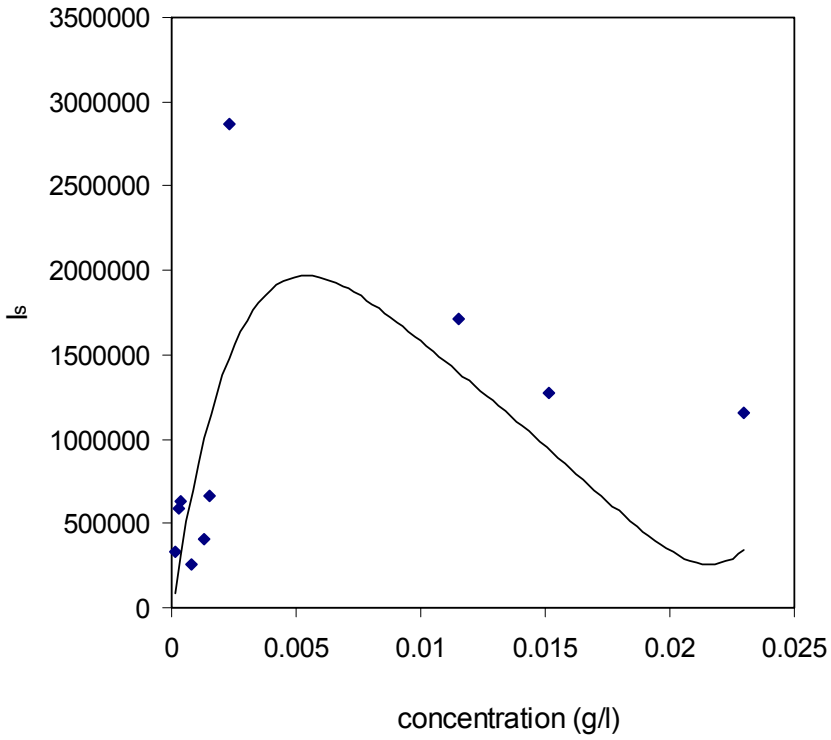

Figure 4.23 Scattering intensity of PVP wrapped SWNT dispersionas a function of concentration at 105°.
Points: experimental data; Line: predicted from Beer-Lambert law

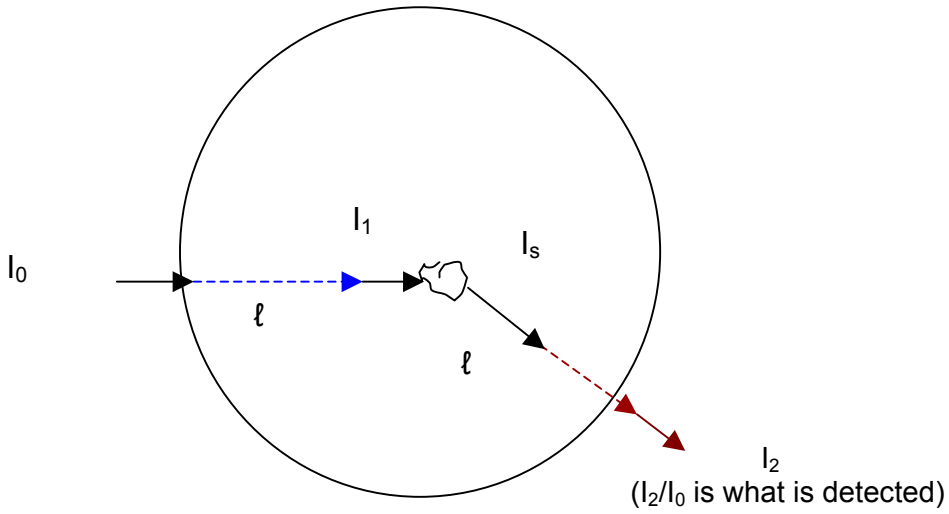

Figure 4.24 light passing through absorptive medium

Based on Beer-Lambert law, I_1 and I_s can be represented by the following equations:

$$I_1 = I_0 \exp(-\varepsilon \ell c)$$

$$I_s = I_2 / \exp(-\varepsilon \ell c)$$

$$I_s / I_1 = [I_2 / \exp(-\varepsilon \ell c)] / I_0 \exp(-\varepsilon \ell c)$$

For single scattering, I_s/I_1 linearly scales with concentration ($I_s/I_1 \sim Kc$, K is constant, c is concentration).

$$Kc = (I_2/I_0)\,[\exp(2\,\varepsilon\,\ell\,c)\}$$

$$\ln (I_2/(I_0\,c)) = \ln K - 2\,\varepsilon\,\ell\,c$$

$$\ln(I_{detect}/c) = \ln K - 2\varepsilon\,\ell\,c$$

$\ln(I_{detect}/c)$ was plotted as a function of concentration c for various angles in Figure 4.25, molar absorption coefficient ε of PVP wrapped SWNT dispersion was determined from the slope (light path is 2.5 cm), which are given as follows:

At 155°, ε = 7.84 E7 l/(mol·cm)

At 90°, ε = 6.52 E+7 l/(mol·cm)

At 75°, ε = 6.76E+7 l/(mol·cm)

At 45 °, ε = 7.04E+7 l/(mol·cm)

On the other hand, the molar absorption coefficient of PVP wrapped SWNT aqueous dispersion can also be estimated based on UV-visible spectrum. Absorption coefficient of SWNT/oleum film at 633 nm was obtained from UV spectrum, which is 35408 cm^{-1}. For PVP wrapped SWNT aqueous dispersion, absorbance of dispersion A is:

$$A = \varepsilon c \ell = \alpha \cdot \ell$$

$$\alpha_{mix} = \alpha_{SWNT} V_{SWNT} + \alpha_{H2O} V_{H2O} + \alpha_{PVP} V_{PVP}$$

where V is volume fraction of component, α is absorption coefficient.

Both absorption from water and PVP can be ignored, the absorption of dispersion comes from SWNTs. The molar absorption coefficient of PVP wrapped SWNT dispersion is calculated as follows:

$$\alpha_{SWNT} V_{SWNT} = \varepsilon_{dispersion} c$$

$$\varepsilon_{dispersion} = 2.66 \text{ E+7 l/(mol·cm)}$$

This value has the same order of magnitude as that from Beer-Lambert law.

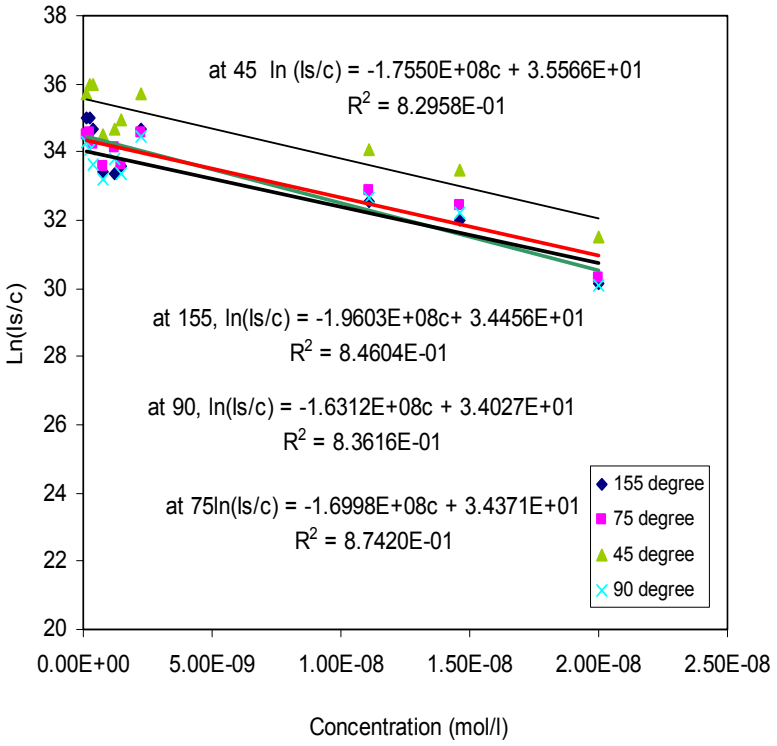

Figure 4.25 Determination of molar absorption coefficient of PVP wrapped SWNT water dispersion.

CHAPTER 5

CONCLUSIONS AND RECOMMENDATIONS

Light scattering technique was used to determine the length of SWNTs in PVP wrapped SWNT aqueous and SWNTs in oleum dispersions. McClain model for long, thin cylinders was used to predict the scattering curves under the effect of extinction coefficient, radius and length of SWNTs, as well as wavelength of incident beam.

It was found that normalized scattering intensity can cancel out the effect of radius and extinction coefficient of SWNTs; the wavelength of incident beam almost does not affect the normalized scattering intensity. The effect of length of SWNTs can be investigated independently. By comparing experimental curve with simulated curves, the average PVP wrapped SWNT length in water was determined to be about 600 nm. The length of SWNTs in oleum could not be determined due to poor data fitting.

There is a critical concentration (C*) in the light scattering behavior of PVP wrapped SWNTs. Below C*, scattering intensity increases with concentration. Above C*, scattering intensity decreases with concentration. By fitting this curve using Beer-Lambert law, the molar absorption coefficient of SWNTs was determined.

Based on the current work, there are several suggestions for the future work. First, sample filtration process should be improved. Centrifugation as well as other methods will be applied to remove impurities; Other SWNT dispersions such as SWNTs/SDS/water and SWNTs/DMSO in which individual tubes are present should be used for light scattering study for SWNT length determination.

REFERENCES

1. PG. Collin, P. Avouis, *Scientific American,* 2000, **283(6)**: 62 - 69
2. E. Hernandex, C. Goze, P. Bernier and A. Rubio, *Phys. Rev. Lett.* 1998, **80**: 4502 - 4505
3. D. Srivastava and Y. W. Chen, *Appl. Mech. Rev*., 2003, **56(2)**: 215 - 230
4. H. D. Wagner, *Chem. Phys. Lett.*, 2002, **361**: 57 - 61
5. T. V. Sreeekumar, T. Liu, B. G. Min, H. Guo, S. Kumar, R.H. Hauge and R. E. Smalley, *Adv. Mater*., 2004,**16(1)**: 58 - 61
6. J. B. Bai and A. Allaoui, Composites part A: *Applied Science and Manufacturing*, 2003, **34**: 689 - 694
7. S. D. Li, Z. Yu, P. Goldde, J. Burke, W. C. Tang, Carbon Nanotube Growth for GHz Devices, http://nano.ece.uci.edu/papers/growth.pdf
8. G. S. Duesberg, J. Muster, V. Krstic, M. Burghard, and S. Roth, *Appl. Phys A*, 1998, **67**: 117 - 119
9. Y. M. Shi and W. M. McClain, *J. Chem. Phys*., 1993, **98(2)**: 1695 - 1711
10. S. Iijima and T. Ichihashi, *Nature*, 1991, **354(7)**: 55 - 58
11. S. Iijima and T. Ichihashit, *Nature*, 1993, **363 (17)**: 603 - 605
12. P. M. Ajayan, J. C. Charlier and A. G. Rinzler, *PNAS*, 1999, **96(25)**: 14199 - 14200
13. M.S. Dresselhaus, G. Dresselhaus and R. Saito, *Carbon*, 1995, **33(7)**: 883 - 891
14. M.S. Dresslhaus, G. Dresselhaus, and P. C. Eklund, *Science of fullerenes and carbon nanotubes*, San Diego, Academic Press, **1996**
15. H. R. Baughman, Science, 2002, **297**: 787 - 789
16. http://www.geocities.com/CapeCanaveral/1320/
17. http://www.mc2link.com/zylon/technical.pdf
18. A. B. Kaiser, *Rep. Prog. Phys*., 2001, **64**: 1 – 49

19. S. Berber, Y. K. Kwon and D. Tomanek., *Phys. Rev. Lett*., 2000, **84 (20)**: 4613 – 4616

20. D. Qian, E. C. Dickey, R. Andrews and T. Rantell, *Appl. Phys. Lett.*, 2000, **76 (20)**: 2868 – 2870

21. X. F. Zhang, T. Liu, T. V. Sreekumar, S. Kumar, V. C. Moore, R. H. Hauge and R. E. Smalley, *Nano. Lett*., 2003, **3(9)**: 1285 -1288

22. W. B. Choi, D. S. Chung, J. H. Kang, H. Y. Kim, I. T. Han, Y. H. Lee, J. E. Jung, N. S. Lee, G. S. Park and J. M. Kim, *Appl. Phys. Lett*., 1999, **75(20)**: 3129 - 3131

23. J. Kong, N. R. Franklin, C. W. Zhou, M .G. Chapline, S. Peng, K.J. Cho, and H. J. Dai, *Science,* 2000, **287**: 622 - 625

24. Y. Saito and S. Uemura, *Carbon*, 2000, **38**: 169 - 182

25. A. C. Dillon, K. M. Jones, T.A. Bekkedahl, C.H. Kiang, D.S. Bethune and M. J. Heben, *Nature*, 1997, **386(27)**: 377 - 379

26. A. Noy, D. V. Vezenov and C. M. Lieber, *Annu. Rev. Mater. Sci*., 1997, **27**: 381 - 421

27. Z. Shao, J.Yang, *Quart. Rev. Biophys*., 1995, **28**: 195 - 251

28. H. J. Dai, J. H. Hafner, A. G. Rinzler, D. T. Colbert, R. E. Smalley, *Nature*, 1996, **384**: 147 - 150

29. E. W. Wong, P. E. Esheehan and C. M. Lieber, *Science*, 1997, **277**: 1971 - 1975

30. P. Poncharal, Z. L. Wang, D. Ugarte and W. A. Deheer, *Science*, 1999, **283**: 1513 - 1516

31. C. V. Nguyen, K. J. Chao, R. Stevens, L. Delzeit, A. Cassell, J.Han and M. Meyyappan, *Nanotechnology*, 2001, **12**: 363 – 367

32. C. M. Lieber, *Solid State Communications*, 1998, **107(11)**: 607 - 616

33. S. Arepalli, P. Nikolaev and W. Holmes, *Appl. Phys. Lett*., 2001, **78(11)**: 1610 - 1612

34. M. Srinivasarao, *Chem. Rev*., 1999, **99**, 1935 - 1961

35. D. W. Schaefer, Science, 1989, **243**, 1023 - 1027

36. W. Zhou, M. F. Islam, H. Wang, D.L. Ho, A. G. Yodh, K. I. Winey and J. E. Fischer, *Chem. Phys. Lett.*, 2004, **384 (1 - 3)**: 185 - 189

37. D.W. Schaefer, J. Zhao, J.M. Brown, D. P. Anderson and D. W. Tomlin, *Chem. Phys .Lett*., 2003, **375**: 369 – 375

38. M. J. Oconnell, P. Boul, L. M. Ericson, C. Huffman, Y. Wang, E. Haroz, C. Kuper, J. Tour, K. D. Ausman and R. E. Smalley*, Chem. Phys. Lett*., 2001, **342**: 265 - 271

39. T. V. Sreekumar, T. Liu, and S. Kumar, *Chem. Mater*., 2003, **15**: 175 – 178

40. Y. M. Shi and W. M. McClain, *J. Chem. Phys*., 1992, **96(11)**: 8086 - 8094

41. C. F. Bohern and D. R. Huffman, *Absorption and scattering of light by small particles*, A wiley - interscience publication, John wiley & sons, **1983**, p52

42. Y. M. Shi, W. M. McClain, *J. Chem. Phys*., 1993, **98(2)**: 1695 - 1711

43. www.function.wolfram.com

44. J. C. Bailar, J. R. Urbana, H. J. Emeleus, S. R. Nyholm, A. F. Dickenson, *Comprehensive inorganic chemistry*, Pergamon press, **1998**, p1261

45. S. Maruyamal, Y. Miyauchi, Y. Murakami and C. Shohei, *New Journal of Physics,* 2003, **5**: 49.1 – 149.12

46. H. C. V. Hulst, *Light scattering by small particles*, NY, John Wiley &Sons Inc., London, **1957,** p5

47. K. A. Stacey, *Light scattering in physical chemistry*, New York academic press inc. publishers, **1956**, p131

48. R. Ghazy, B. El. Baradie, A. El. Shaer, F. El. Mekawey, *Optics and Laser Technology*, 1999, **31**: 447 – 453

49. M. Patricia, A. Patterson and A. M. Jamieson, *Macromolecules*, 1985, **18**: 266 - 212

50. S. P. Parker, *McGraw - Hill encyclopedia of physics*, McGraw hill inc., **1996**, p8